Interannual variability of Greenland winter precipitation sources: 2. Effects of North Atlantic Oscillation variability on stable isotopes in precipitation

H. Sodemann, Valérie Masson-Delmotte, C. Schwierz, B. Vinther, H. Wernli

Interannual variability of Greenland winter precipitation sources: 2. Effects of North Atlantic Oscillation variability on stable isotopes in precipitation

H. Sodemann,[1,2] V. Masson-Delmotte,[3] C. Schwierz,[1,4] B. M. Vinther,[5] and H. Wernli[6]

Received 25 September 2007; revised 6 February 2008; accepted 17 March 2008; published 25 June 2008.

[1] A new Lagrangian moisture source diagnostic is applied to identify the atmospheric conditions relevant for the fractionation of stable water isotopes during evaporation over the ocean and subsequent transport to Greenland. Northern Hemisphere winter months with positive and negative North Atlantic Oscillation (NAO) index are studied on the basis of ERA-40 reanalysis data. Diagnosed moisture transport conditions are supplied to a Rayleigh-type isotope fractionation model to derive estimates for the isotopic composition of stable isotopes in winter precipitation on the Greenland plateau for the two NAO phases. Because of changes in atmospheric circulation, moisture source locations for precipitation in Greenland vary strongly for different phases of the NAO. The mean source SST is ~5.0 K warmer during negative NAO months compared to the positive phase. This signal is considerably stronger than what would result from interannual SST variability at a spatially fixed moisture source. Furthermore, moisture transport takes place at warmer temperatures during NAO negative conditions. Simulated average isotopic depletion of Greenland precipitation is less negative by 3.8 ± 6.8‰ for $\delta^{18}O$ during the negative compared to the positive NAO phase. Comparison with ice core data from central Greenland for three winters shows good agreement between observed and simulated variability. The synoptic interplay of the initial conditions at the moisture sources and of the atmospheric transport conditions leads to enhanced NAO-related interannual variability of stable isotopes. This could be important for understanding rapid shifts in stable isotopes during past climates. The isotope modeling applied here, however, considerably underestimates the absolute level of isotopic depletion. The offset is attributed to approximations in the model and uncertainties in the comparison with observational data. The high spatial resolution of the Lagrangian method reveals the nonhomogeneous structure of isotope NAO variability over the Greenland ice sheet. The results are therefore potentially useful for selecting new ice core drilling sites with maximum NAO variability.

Citation: Sodemann, H., V. Masson-Delmotte, C. Schwierz, B. M. Vinther, and H. Wernli (2008), Interannual variability of Greenland winter precipitation sources: 2. Effects of North Atlantic Oscillation variability on stable isotopes in precipitation, *J. Geophys. Res.*, *113*, D12111, doi:10.1029/2007JD009416.

1. Introduction

[2] Stable water isotopes in precipitation are used as an observational method to gain understanding of the atmospheric hydrological cycle [*Dansgaard*, 1964; *Rozanski et al.*, 1982]. During evaporation and condensation, heavy isotopes are preferentially enriched in the condensed phase. A precipitating air mass will be continuously depleted of heavy isotopes in the remaining water vapor. This atmospheric isotope fractionation process is also known as isotopic distillation. As isotopic distillation depends strongly on the air temperature (mainly due to the saturation vapor pressure, but also the temperature dependency of the fractionation factors), the level of isotopic depletion of water vapor and precipitation are testimony to its evaporation source and the transport conditions. More specifically, the influences on the isotopic composition of an air mass

[1]Institute for Atmospheric and Climate Science, ETH Zurich, Zurich, Switzerland.
[2]Now at Norwegian Institute for Air Research, Kjeller, Norway.
[3]LSCE, IPSL, CEA, CNRS, UVSQ, Gif-sur-Yvette, France.
[4]Now at Institute for Climate and Atmospheric Science, University of Leeds, Leeds, UK.
[5]Centre for Ice and Climate, Niels Bohr Institute, University of Copenhagen, Copenhagen, Denmark.
[6]Institute for Atmospheric Physics, University of Mainz, Mainz, Germany.

0148-0227/08/2007JD009416

include the initial isotopic composition of the ocean water; temperature, humidity, and wind speed during evaporation, and after initial condensation also the air temperature evolution within the cloud [*Craig and Gordon*, 1965; *Merlivat and Jouzel*, 1979]. Additional processes, such as convection, mixing with ambient water vapor and evaporating precipitation can also alter the isotopic composition. The level of enrichment or depletion of stable water isotopes (HDO and $H_2^{18}O$) is commonly expressed in the δ notation, relative to Vienna standard mean ocean water. Values for δD and δ^{18}O (in ‰) close to zero are typical for ocean surface water. The average isotopic ratios measured in precipitation and water vapor are generally negative, lower for snow than for rain, and decrease with increasing latitude [*Dansgaard*, 1964; *Rozanski et al.*, 1993]. Lowest values are observed at the polar ice caps [*Jouzel et al.*, 1983; *Fujita and Abe*, 2006; *Masson-Delmotte et al.*, 2008].

1.1. Isotope Paleothermometer and the Role of the Moisture Sources

[3] One of the most important applications of stable isotopes in the water cycle is their use for the reconstruction of past climate variability, on interannual to multimillennial timescales. A primary tool for the paleoclimatic interpretation of stable isotope records is the empirical isotope-temperature ($\delta-T$) relationship established by *Dansgaard* [1964]. The climatological latitudinal (and annual mean temperature) gradient of stable isotopes in precipitation are thereby used for the reconstruction of the temperature changes during past climate shifts, such as glacial-interglacial cycles, from Greenland and Antarctic ice cores [*Dansgaard et al.*, 1993; *NorthGRIP Members*, 2004; *EPICA Community Members*, 2004].

[4] A major complication of the $\delta-T$ relationship however is that Greenland temperature reconstructions for the last glacial maximum are $\approx$10 K warmer for stable isotope based reconstructions compared to bore hole temperatures [*Cuffey et al.*, 1995; *Cuffey and Clow*, 1997; *Dahl-Jensen et al.*, 1998]. The same also holds true for abrupt temperature changes in the past [*Masson-Delmotte et al.*, 2006, and references therein]. Hypotheses put forward to reconcile this discrepancy suggest changes in the precipitation seasonality [*Steig et al.*, 1994; *Krinner et al.*, 1997; *Krinner and Werner*, 2003], in the surface inversion above Greenland [*Jouzel et al.*, 1997; *Hoffmann et al.*, 2000], or in ice sheet elevation [*Johnsen et al.*, 1995]. Several studies in addition point to the potential of moisture source changes and, therefore, changes in sea surface temperature (SST) during evaporation, and the initial isotopic composition for resolving this discrepancy [*Jouzel et al.*, 1997; *Boyle*, 1997; *Masson-Delmotte et al.*, 2005a].

[5] A second-order isotope parameter which is often used to gain information on the moisture source conditions is the Deuterium excess (*d* excess). The *d* excess is defined as the deviation of the relative fractionation strength of δ^{18}O and δD from the value that would be achieved under equilibrium conditions ($d = \delta D - 8 \cdot \delta^{18}O$ [*Dansgaard*, 1964]). It is a measure for so-called kinetic effects or nonequilibrium fractionation, which are caused by the different molecular diffusivities of the HDO and $H_2^{18}O$ molecules. Nonequilibrium fractionation is thought to mainly take place during evaporation (influenced by wind speeds and relative humidity (RH) directly above the ocean surface), but also in supersaturated mixed phase clouds, or during cloud droplet reevaporation [*Dansgaard*, 1964; *Ciais and Jouzel*, 1994; *Jouzel et al.*, 2007]. Since the slope 8 in the definition of the *d* excess depends on the temperature during isotopic distillation, equilibrium fractionation can also induce changes in the *d* excess, in particular with regard to equilibrium fractionation factors for ice.

[6] The moisture sources of Greenland, and the associated source SSTs have been addressed in several previous studies. Using a simple isotope fractionation model, *Johnsen et al.* [1989] concluded that annual mean moisture sources for Greenland should be located at 35–40°N with corresponding source region SSTs of ~22–26°C (but noting that colder source SST would exist during winter). *Barlow et al.* [1993] interpreted interannual variability in the *d* excess at Summit as a signal of SST variability at the moisture source at 30–40°N. *White et al.* [1997] assumed an annual mean moisture origin at a latitude band of 20–30°N, while *Jouzel and Koster* [1996] and *Barlow et al.* [1997] argued for more northerly, and therefore 5–10 K colder moisture sources. For the winter season, the importance of midlatitude and polar moisture sources was also supported by tagging and isotope-tagging GCM studies [*Charles et al.*, 1994; *Werner et al.*, 2001].

[7] While *d* excess is often used as an indicator of SST and RH at the moisture source [*Jouzel and Merlivat*, 1984; *Johnsen et al.*, 1989; *Barlow et al.*, 1993], in light of recent insight into the variability of moisture source regions, it is increasingly recognized that moisture source changes (associated with changes in atmospheric circulation) could also exert an influence on the *d* excess [*Masson-Delmotte et al.*, 2005a, 2005b]. Hence, while the *d* excess appears to have a great potential for paleoclimate reconstructions, the interpretation of this parameter remains complex.

[8] For a full understanding, knowledge of all mechanisms influencing the *d* excess, as well as the deconvolution of influences from evaporation versus atmospheric transport are required. Part 1 of this paper series [*Sodemann et al.*, 2008] (hereinafter referred to as SSW08) is the first attempt to diagnose Greenland's moisture sources during winter from reanalysis data. This provides the opportunity to directly investigate the influence of moisture source changes on stable isotope variability.

1.2. Interannual Variability of Stable Isotopes

[9] On seasonal to interannual timescales, stable isotope data from Greenland exhibit significant variability. The North Atlantic Oscillation (NAO) is an important (mainly atmospheric) mode of variability in the Northern Hemisphere (see SSW08 and references therein). For different winters, it is associated with marked changes in circulation, temperature, and precipitation over Greenland. NAO-induced variability is therefore apparent in the snow accumulation sequence of ice cores [*Appenzeller et al.*, 1998a, 1998b; *Mosley-Thompson et al.*, 2005], as well as to some extent in the (winter) stable isotope signals in firn and ice cores from central Greenland [*Barlow et al.*, 1993, 1997; *White et al.*, 1997]. The *d* excess also exhibits seasonal and interannual variability in Greenland firn and ice core records [*Fischer et al.*, 1995; *Hoffmann et al.*, 1998a].

[10] Stable isotope records can be used to reconstruct time series of Greenland temperatures several centuries beyond the period of meteorological observations, for example as part of multiproxy reconstructions of the NAO [*Vinther et al.*, 2003]. Even though the NAO explains about half of the atmospheric variability above Greenland during winter [*van Loon and Rogers*, 1978], it only explains about ~26% of the variance observed in (spatially limited) stable isotope records [*Rogers et al.*, 1998; *Vinther et al.*, 2003]. *Vinther et al.* [2006] found that the temperature record from several coastal Greenland stations can explain about 56% of the winter $\delta^{18}O$ variance in a set of 7 Greenland ice cores. Yet, the spatial coverage of Greenland ice core data is far from complete. Furthermore, it is currently not fully understood by which physical mechanisms the NAO imprints on the stable isotope signal in Greenland precipitation. A better understanding of the physical basis of the variability can have fundamental implications for the interpretation of signals of past climate variability observed in Greenland.

1.3. Stable Isotope Models

[11] All of the above prompts for a better understanding of stable isotope processes on short timescales that integrate to the climatological stable isotope record. To this end, isotope fractionation of HDO and $H_2^{18}O$ has been incorporated in models of various degrees of complexity. Isotope general circulation models (GCMs) comprise all known fractionation effects during phase changes to simulate stable water isotopes on a global scale [*Joussaume et al.*, 1986; *Hoffmann et al.*, 1998b; *Schmidt*, 1999; *Noone and Simmonds*, 2002]. The climatological mean isotopic composition of surface precipitation can be simulated successfully with these models. Apart from supporting the interpretation of stable water isotopes in ice cores and other observations, this allows also to use stable isotopes as a means to evaluate the realism of the water cycle in GCMs. Comparison to observed atmospheric variability on daily to monthly timescales is however not possible with such models. Ongoing efforts to address shorter timescales include GCM simulations nudged to atmospheric reanalysis data [*Noone*, 2006; G. Hoffmann, personal communication, 2007]; and the development of mesoscale atmospheric models with isotope fractionation processes [*Sturm et al.*, 2005].

[12] Lagrangian models driven by meteorological (re)-analysis data offer the potential to simulate the isotopic composition of specific precipitation events. Lagrangian isotope models have long been used to calculate isotopic fractionation along idealized air mass trajectories for moisture transport to Antarctica and Greenland [*Jouzel and Merlivat*, 1984; *Johnsen et al.*, 1989; *Petit et al.*, 1991; *Ciais and Jouzel*, 1994; *Ciais et al.*, 1995]. More recently, Lagrangian box models were applied to trajectories based on reanalysis data over Antarctica [*Schlosser et al.*, 2004; *Helsen et al.*, 2004, 2005, 2007]. So far, Lagrangian models have not been used with diagnosed moisture sources for Greenland. Information on the moisture source conditions are however crucial for initializing Lagrangian isotope models [*Jouzel and Koster*, 1996; *Delmotte et al.*, 2000].

[13] In this study, we attempt to model the mean isotopic composition of Greenland precipitation during winter from a large number of individual precipitation events. The model approach is based on conditions of isotopic fractionation during water vapor transport in the atmosphere, diagnosed from reanalysis data. We thereby aim to disentangle the factors which lead to the observed NAO variability of precipitation isotopes. For this purpose, we apply the Lagrangian moisture source and transport diagnostic in the same configuration as presented in part 1 (SSW08). As this study is based on reanalysis data, a direct comparison with present-day stable isotope observations from Greenland ice cores and snow pits can be conducted. Also, the high spatial resolution allows to identify the spatial pattern of the isotopic variability on the Greenland plateau, and to consider regions where currently no ice core data is available.

[14] In the remainder of this paper, we first extend the method of SSW08 to diagnose the conditions at the evaporation sites and during atmospheric transport of water vapor which are relevant for isotopic distillation (section 2). On the basis of the findings presented in section 3, we apply a Rayleigh-type Lagrangian isotopic fractionation model [*Ciais and Jouzel*, 1994], using the diagnosed moisture transport conditions to predict the isotopic composition of the precipitation in Greenland (section 4). Key implications of the results are further discussed in section 5, and conclusions given in section 6.

2. Methods

2.1. Diagnosed Fractionation Conditions

[15] The conditions of isotopic distillation were extracted using the Lagrangian moisture transport diagnostic of SSW08. The same calculation setup as in SSW08 was used to diagnose the transport conditions of moisture on the way to Greenland along its atmospheric transport path. To this end, a large number of three-dimensional kinematic backward trajectories was calculated backward in time for 20 days from the location of the air mass above the Greenland ice sheet (defined here as the area above 2000 m a.s.l.). Calculations were carried out for 30 selected winter months from the ERA-40 period (1959–2002), of which 10 each had a pronounced positive, negative, and near-zero NAO index. For each precipitation event over the Greenland ice sheet, air parcels were traced at 6 h time resolution, starting at ~6000 horizontally and vertically distributed locations within the air mass. Further details on the calculation setup are available in SSW08.

[16] All conditions concerning the moisture transport were extracted from ECMWF's ERA-40 reanalysis data halfway along 6 h trajectory segments. The respective conditions at this intermediate location at $t + 3$ h were linearly interpolated in time between t and $t + 6$ h. In addition to the parameters extracted for the study of SSW08 (latitude, longitude, pressure, potential temperature, specific humidity at the air parcel location), the following parameters were diagnosed here:

[17] 1. For the evaporation conditions, SST over water (skin temperature SKT over land), 2 m air temperature (T_{2m}), RH, and 10 m wind velocity (U_{10m}) at each moisture uptake location were diagnosed (Figure 1, label 1). These parameters are typically used to characterize the evaporation conditions at the moisture source [*Craig and Gordon*, 1965; *Merlivat and Jouzel*, 1979].

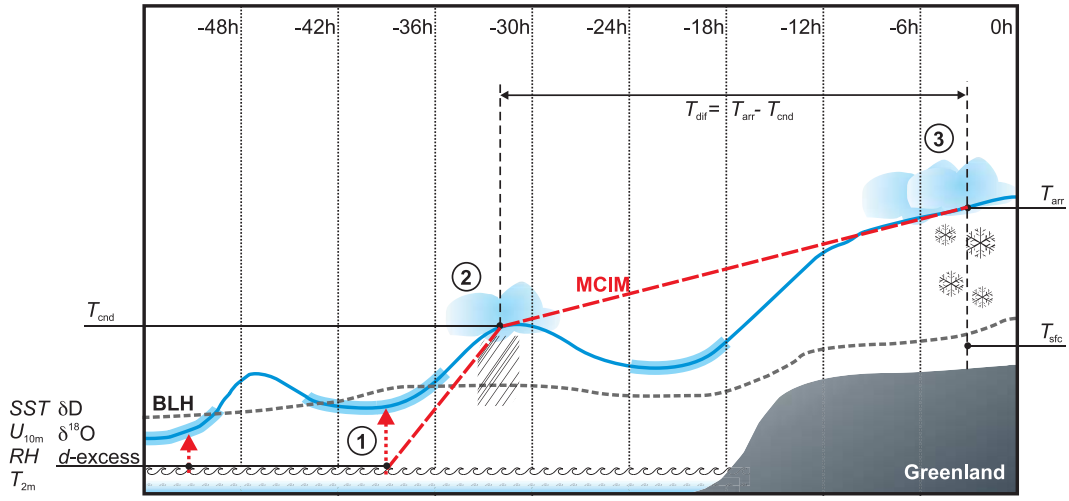

Figure 1. Sketch of the definition of temperatures affecting the isotopic fractionation process along a backward trajectory (blue line). Time before arrival is shown at the top. BLH, boundary layer height. Blue highlighted sections along the trajectory denote sections of moisture increase, i.e., moisture uptake. Dashed red line shows the idealized fractionation trajectory of the MCIM model. See text for details.

[18] 2. For the initial condensation conditions, the horizontal and vertical location, and the temperature (T_{cnd}) where clouds begin to form were recorded for each air parcel. This initial condensation was identified where an air parcel reached for the first time more than 80% RH after its last moisture uptake (Figure 1, label 2). The 80% threshold was adopted since the cloud parameterizations in the ECMWF model allow for subgrid-scale condensation and cloud formation above this threshold.

[19] 3. For the cloud arrival conditions, temperature (T_{arr}) and pressure (p_{arr}) of precipitating air parcels were extracted for each precipitation event above the Greenland ice sheet. Cloud structures may be represented by air parcels at several vertical levels. In addition, the 2 m air temperature at the corresponding surface location (T_{sfc}) was retrieved (Figure 1, label 3). In almost all cases, minimum saturation vapor pressure during transport was reached at the arrival location of the precipitating air parcel. This location is therefore considered as the terminal point of the isotopic distillation.

[20] All diagnosed parameters were then composited, weighted with the air parcel's contribution to precipitation in Greenland (see below). The absolute temperatures at which the isotopic distillation takes place (between T_{cnd} and T_{arr}) strongly influence the fractionation via the corresponding saturation vapor pressure. In addition, the temperature range $T_{dif} = T_{arr} - T_{cnd}$ determines the extent of isotopic equilibrium fractionation in $p-T$ space [*Dansgaard*, 1964; *Jouzel et al.*, 1997]. The larger T_{dif}, the more isotopic distillation can occur, and the more depleted will the final isotopic composition of the moisture be.

[21] As a caveat, note that the effects of vertical moisture redistribution due to convection and precipitation evaporation, as well as mixing with surrounding air are not captured by our methodology. On the basis of the moisture source attribution of SSW08, about 66% of the water vapor that contributed to Greenland precipitation could be assigned to specific evaporation areas. Convective moisture transport is not explicitly determined by their source attribution model. However, from the amount of moisture that was diagnosed as entering the air parcels above the boundary layer, SSW08 estimated this contribution to be in the order of 20%. For the remaining 14%, no definitive moisture source could be identified (SSW08).

2.2. Isotopic Fractionation From Diagnosed Parameters

[22] In order to estimate the isotopic composition of each precipitation event, the Mixed-Cloud Isotope Model (MCIM) [*Ciais and Jouzel*, 1994] was run with the diagnosed evaporation and fractionation conditions. MCIM is a zero-dimensional Rayleigh-type isotope model with parameterized mixed phase microphysical processes. MCIM calculates fractionation along an idealized $p-T$ trajectory, based on specified evaporation and arrival temperatures. In the original standard setup, the condensation temperature is calculated by adiabatically lifting an air parcel from the sea surface to its lifting condensation level (LCL). Rayleigh fractionation is then calculated along a moist adiabat until the point (T_{arr}, p_{arr}) is reached. Thereby, T_{arr} is given by an empirical relation between temperatures inside the typically strong surface inversion in polar regions, and the free troposphere above (see Appendix A).

[23] In this study, isotope fractionation was calculated individually for each air parcel precipitating over Greenland, using the identified fractionation conditions. Fractionation was calculated in the respective diagnosed temperature range from T_{cnd} to T_{arr}. Consistency with the MCIM calculation procedure required a modified lapse rate and surface RH to be used, which led to an LCL that coincided with the diagnosed initial condensation conditions (see section 2.1). Figure 1 shows the MCIM fractionation trajectory (dashed red line) that corresponds to the diagnosed air parcel trajectory (blue line). For the initial isotopic composition, data from the ECHAM4 isotope GCM were used (see section 2.3 below). As a further modification to the standard MCIM setup, diagnosed cloud arrival temperatures T_{arr} were directly supplied to MCIM. Otherwise, the same setup as described by

Masson-Delmotte et al. [2005b] was applied (see Appendix A for a more detailed description of the modifications).

[24] The isotopic composition δ_{arr} of a particular 6-hourly precipitation event at a certain location on the calculation grid over Greenland with precipitation P_{arr} was calculated as a weighted average from all contributing moisture sources on all relevant levels of the troposphere. More specifically, the contribution δ^j_{arr} of one air parcel with precipitation P^j, if associated with N moisture sources, was calculated as the composite of each source's contribution δ^i, weighted by the respective contribution factors f^i (SSW08):

$$\delta^j_{arr} = \frac{\sum_{i=1}^{N} \delta^i \cdot f^i}{\sum_{i=1}^{N} f^i}, \quad (1)$$

whereby $\sum_{i=1}^{N} f^i \leq 1$. Similarly, the contributions from all M air parcels in an atmospheric column that contribute to P_{arr} were averaged to obtain the isotopic composition δ_{arr} of a 6-hourly precipitation event at a specific site:

$$\delta_{arr} = \frac{\sum_{j=1}^{M} \delta^j_{arr} \cdot P^j}{\sum_{j=1}^{M} P^j}, \quad (2)$$

whereby $\sum_{j=1}^{M} P^j = P_{arr}$. This procedure was performed every 6 hours, separately for all locations with precipitation on the calculation grid over the Greenland plateau (SSW08, Figure 2). Mean fields were then calculated both for the 30 individual months and for the NAO+ and NAO− phases, using the same averaging as in equation (2).

2.3. Initialization With GCM Isotope Data

[25] A crucial problem of Lagrangian Rayleigh fractionation models concerns the initial isotopic composition of the water vapor at the evaporation site. Lacking directly measured isotopic composition of evaporating water vapor at sufficient spatial resolution, *Merlivat and Jouzel* [1979] used a global closure equation for the original MCIM model. *Jouzel and Koster* [1996] showed this global closure to be inconsistent with observations. Instead, they recommended to use the stable isotope composition at the lowest layer of isotope GCMs as initial values for Lagrangian isotope models. This was also confirmed in a study comparing MCIM simulations initialized with the global closure equation and surface vapor from an isotope GCM for coastal Antarctica [*Delmotte et al.*, 2000].

[26] Therefore, in addition to evaporation parameters at the moisture sources, we retrieved the corresponding isotopic composition of the surface vapor from a simulation with the ECHAM4 isotope GCM [*Hoffmann et al.*, 1998b; *Werner et al.*, 2001]. Gridded $2^\circ \times 2^\circ$ monthly mean data were acquired from the SWING database (SWING database accessed in November 2005 at http://atoc.colorado.edu/~dcn/SWING/index.php) for the required months. We used a simulation of present-day conditions from the ECHAM4 isotope GCM, which covers a 134-year period driven by the monthly HadISST data V1.1 at T159L30 resolution (experiment S1B). The HadISST data is based on monthly observations and hence contains realistic interannual variability [*Rayner et al.*, 2003]. In general, despite a small warm bias in Greenland surface temperatures, ECHAM4 simulates a reasonable annual mean level of stable isotopes and a realistic seasonal amplitude (G. Hoffmann, personal communication, 2007). Isotopic fractionation during evaporation in the ECHAM4 isotope GCM depends on local conditions for air temperature, RH, surface winds, and SST according to a linear resistance model [*Craig and Gordon*, 1965; *Hoffmann et al.*, 2000]. We extracted the isotopic composition (δD, δ^{18}O) in the lowest model layer at each diagnosed moisture source location (Figure 1, label 1). The isotope values of the surface vapor were then supplied as initial conditions to the MCIM isotope fractionation model, as described in the previous section.

2.4. Comparison With Stable Isotope Observations From Greenland

[27] In order to relate the modeled isotope values to in situ observations, a comparison with stable isotope data from sites in southern central Greenland was carried out. Three periods were considered where (1) trajectories had been calculated for at least two consecutive months from a winter season (DJF) and (2) ice core data with sufficiently high temporal resolution were readily available. It was essential to choose ice core data from an area with sufficiently high accumulation to resolve winter rather than annual mean conditions.

[28] On the basis of these criteria, the Alphabet drilling sites [*Clausen et al.*, 1988] were selected. The shallow Alphabet cores were drilled in an inverse L-shaped array southeast of the drilling site Crête in central Greenland (70.63–71.76°N; 35.82–39.62°W, 3018–3138 m a.s.l.). Distances between cores were about 30–80 km, and the annual mean δ^{18}O value was -34.1 ± 1.0‰ [*Clausen et al.*, 1988]. Winter season isotope signals were calculated from an average of the back-diffused δ^{18}O values [*Johnsen et al.*, 2000] of five cores (A, B, D, E, and G). *Fischer et al.* [1995] estimated that 50–60% of the annual accumulation in the area is deposited during the winter half year. Here, winter was defined as 35% of the annual accumulation, centered around the lowest δ^{18}O value. Significant differences exist between the five cores, with a mean winter difference of 1.27‰, and a signal-to-noise ratio of 0.52 for the seasonal δ^{18}O.

[29] The chosen winter periods were 1968/1969 and 1983/1984 (2 months each) and 1964/1965 (3 months). Data for winter 1983/1984 was not covered by the shallow cores and therefore taken from nearby snow pit data. Postdepositional diffusion smoothes out the high-frequency variability from the ice core data which would be present in precipitation data (and, to a lesser degree, in snow pit data). The ice core data (typically 1–2 data points per ice core and winter) were compared with a seasonal average of the modeling results for 9 grid points of the trajectory calculation grid which are within a range of 50 km from the drilling sites.

3. Diagnosed Fractionation Conditions

[30] The fractionation conditions that result from the Lagrangian moisture diagnostic are presented in the logical sequence of moisture transport: Evaporation conditions are shown first, followed by the initial condensation locations. Then the arrival conditions of the water vapor above the

Greenland ice sheet are presented, as well as the corresponding temperature conditions at the surface.

3.1. Evaporation Conditions

[31] Figure 2a shows the mean SST in the North Atlantic for the 30 winter months considered. The overlaid contour lines mark the main moisture source areas for Greenland precipitation during the two NAO phases (SSW08). Figure 2a indicates qualitatively that the moisture source temperatures vary strongly with the NAO because of the shifted location of the main moisture source. The histogram of the moisture source temperatures (Figure 3a) shows the striking difference in the mean moisture source SST with ~5.0 K warmer conditions during the NAO− phase (NAO+ mean and standard deviation: 5.0 ± 6.5°C, NAO−: 10.0 ± 6.7°C). During NAO+ conditions most moisture evaporates at SSTs below 8°C, while during the NAO− phase a considerable share of the moisture originates at SSTs above 12°C. Such strong SST changes within different winter months could not be induced by local SST variability alone.

[32] Figure 4a shows the regional differences in moisture source SST as Lagrangian forward projections (LFPs) onto the respective arrival locations at the Greenland plateau. The LFPs from the individual trajectories are weighted by their contribution to the local grid point precipitation. For the NAO+ phase, the precipitation at the fringe of the Greenland plateau evaporated on average at SSTs of 3–6°C (Figure 4a, left). The higher interior of the plateau is associated with warmer source region SSTs (8–11°C). During the NAO− phase instead, the moisture originating from the warmest ocean areas precipitates in the northeast (12–15°C, Figure 4a, middle). More southerly areas are in this NAO phase associated with source SSTs of 9–12°C. The shifted location of the area associated with warmest source region SSTs on the Greenland plateau could result from transport changes: relatively more short-range advection occurs during NAO+ months, while long-range transport is more frequent during NAO− months (SSW08). Hence, source region SST for the northeast of the plateau varies by ~6–10 K with the NAO. Most other areas experience only a shift of 2–6 K (Figure 4a, right). NAO variability of the source SSTs is lowest for precipitation in the central western plateau (~2 K).

[33] The patterns of the source SST (Figure 4a) resemble the distribution of source latitudes over the Greenland ice sheet (SSW08, Figure 9b). For T_{2m} at the evaporation locations, the pattern is very similar to that of the SST, yet with an almost uniform negative offset of ~3 K (not shown). Mean RH above the evaporation areas is 72.5 ± 9.5% for the NAO+ and 71.2 ± 9.5% for the NAO− phase. The LFP patterns for RH at the evaporation site are rather similar for the two NAO phases (not shown).

[34] Surface winds at the moisture sources are an important driver for evaporation, and can influence the *d* excess. During the NAO+ phase, 10 m wind velocities at the evaporation sites (U_{10m}, Figure 4b, left) are rather high for precipitation that falls along the east coast of Greenland (11–13 m s^{-1}), and markedly lower (8–10 m s^{-1}) for precipitation at the west coast (overall mean 11.1 ± 4.7 m s^{-1}). For the NAO− phase, mean evaporation winds are uniformly distributed and around 9.8 ± 4.0 m s^{-1} (Figure 4b, middle). The LFP patterns of U_{10m} are similar to the LFPs of the source longitudes (SSW08, Figure 8b). The relatively higher wind velocities at the evaporation sites during the NAO+ phase probably reflect the concurrent higher storminess in the western North Atlantic. It remains however unclear why precipitation over the western plateau of Greenland is associated with lower evaporation wind speeds.

[35] We emphasize again that our findings for the winter season contrast to some extent with earlier studies that assumed a geographically fixed annual mean moisture source for Greenland (see discussion in SSW08). At least for the winter season, our results support the perspective obtained from several GCM studies that Greenland is associated with multiple geographically separated moisture sources [*Schmidt et al.*, 2007]. This finding is also consistent with Holocene records of *d* excess from the GRIP and NorthGRIP ice cores [*Masson-Delmotte et al.*, 2005a]. The spatial variability of moisture sources causes an interannual variability of moisture source SSTs during winter which is more pronounced than expected previously.

3.2. Initial Isotopic Composition

[36] Initial values for the isotopic fractionation of the water vapor are diagnosed from output of the ECHAM4 isotope GCM (see section 2.3). Figures 2b–2d show the mean stable isotope composition of water vapor at the lowest model level over the North Atlantic during the considered winter months. Values in the North Atlantic range between −85‰ to −150‰ for δD and −12‰ to −20‰ for δ^{18}O. These values directly result from the GCM parameterizations for isotopic fractionation during evaporation, but also from the mixing with ambient moisture in the model [*Armengaud et al.*, 1998]. Both, δD and δ^{18}O exhibit a mainly meridional gradient across the North Atlantic, which is indicative of the strong influence of SST on these quantities (Figures 2b and 2c). As with SST, the isotope gradient is weaker in the eastern North Atlantic. Mean surface values for *d* excess are in the range of ~5–15‰ (Figure 2d). The meridional *d* excess gradient is strongest in the western North Atlantic, and weakens toward the east. Both the surface water isotopes and the sea level pressure of the ECHAM4 simulation have almost no NAO variability for the considered winter months (not shown). Since the initial isotopic composition of the water vapor is mainly determined by the HadISST, we assume that the lacking atmospheric variability does not overly affect the surface values of δD and δ^{18}O. Analysis of the short-term variability of the surface variables in isotope GCMs could clarify to what extent this assumption is indeed justified [*Hoffmann et al.*, 1998b].

[37] Lagrangian forward projections of the diagnosed isotopic composition of the evaporating water vapor have patterns similar to the SST (Figures 4c and 4d). This again demonstrates the control of SST over the isotopic composition close to the surface. For the NAO+ (NAO−) phase, mean initial values and standard deviations are −138 ± 23‰ (−124 ± 23‰) for δD (Δ δD = 14.1‰), and −18.4 ± 2.9‰ (−16.7 ± 2.8‰) for δ^{18}O (Δ δ^{18}O = 1.7‰). The NAO variability of source region δD and δ^{18}O is strongest in the northeast of the Greenland plateau and along the southern ridge (Figures 4c and 4d, right). Maximum vari-

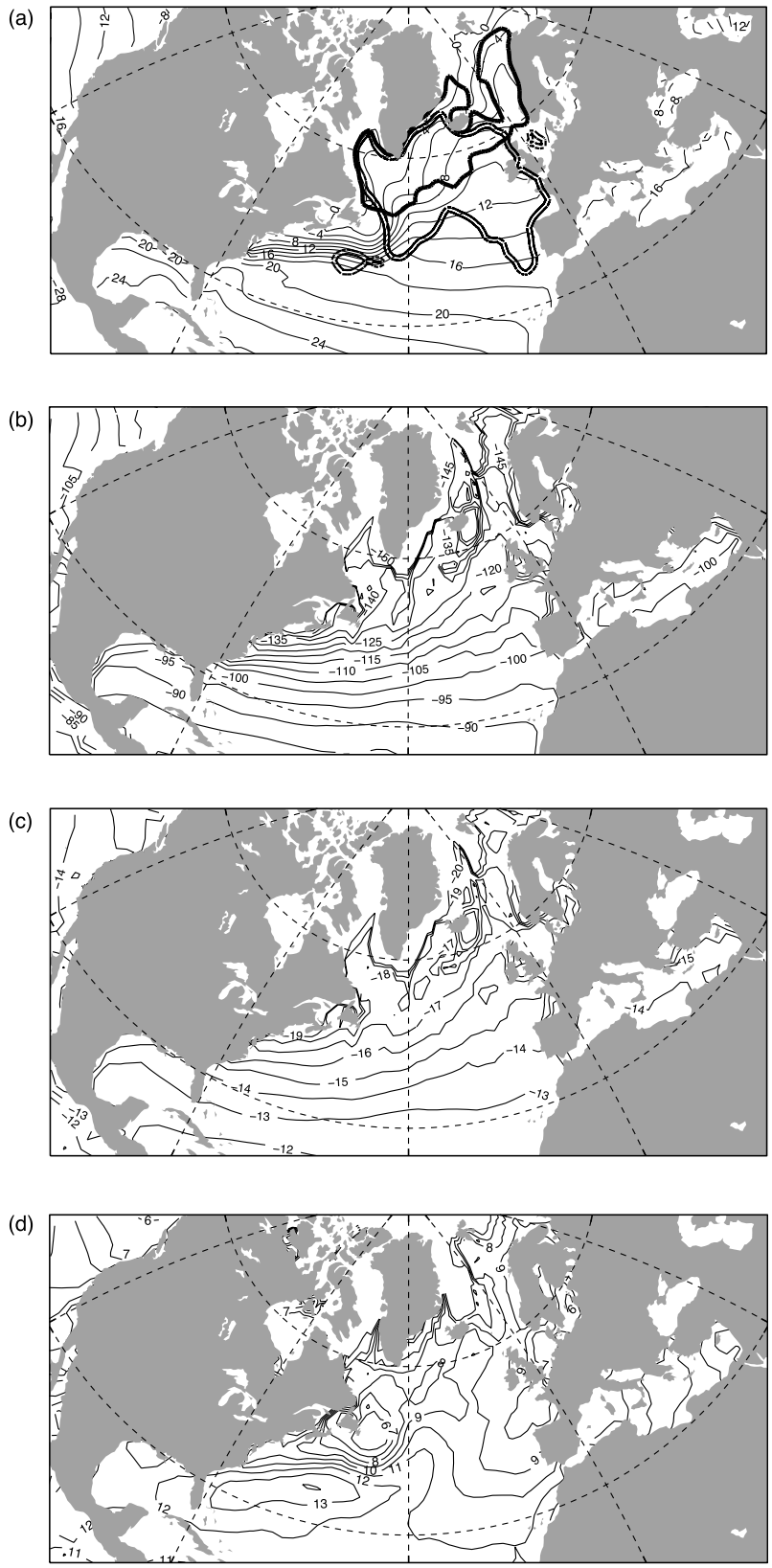

Figure 2. Winter mean conditions of (a) SST from ERA-40 and the stable isotope parameters (b) δD (‰), (c) δ^{18}O (‰), and (d) *d* excess (‰) at the lowest layer of the ECHAM4 isotope model, averaged over the selected 30 winter months. Data in Figures 2b–2d are from monthly mean files of the SWING database. Some contours in Figures 2b–2d have been deleted for clarity. Bold contours in Figure 2a are the moisture source regions for the NAO+ (single) and NAO− phase (double), delineated at 20% of the respective moisture uptake maximum values.

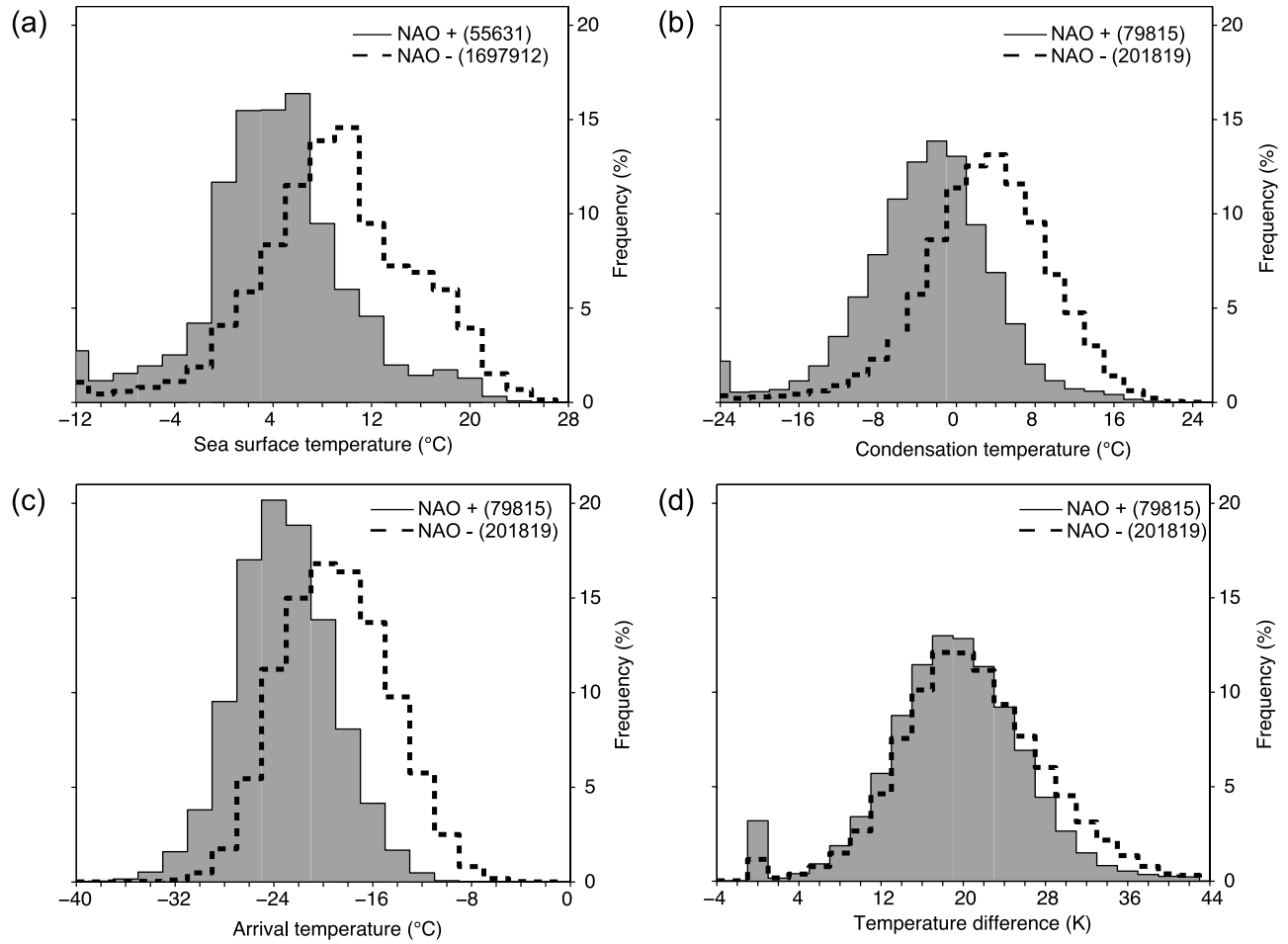

Figure 3. Histograms of (a) moisture source SST (°C) for each evaporation location, weighted by the respective contribution to precipitation in Greenland, (b) initial condensation temperature T_{cnd} (°C), (c) arrival temperature T_{arr} (°C), and (d) temperature difference T_{dif} (K) diagnosed for each precipitating trajectory and weighted by the respective precipitation amount. Figures in brackets give the number of data used for the histograms.

ability for the two isotopic species amounts to ~20‰ and ~3‰, respectively.

[38] The *d* excess projected from the moisture sources to the arrival points over Greenland gives on average 8.6 ± 2.9‰ for the NAO+ phase and 9.2 ± 2.5‰ (Δd excess = 0.6‰) for the NAO− phase (Figure 4e). For the NAO+ phase, more spatial variability is apparent. The LFP pattern of *d* excess for the two NAO phases approximately shows an inverse relation to the evaporation wind speeds (Figure 4b). This inverse relationship is particularly evident in the respective NAO variability plots (Figures 4b and 4e, right). In addition, there is a weak positive correlation between the moisture source SST and the *d* excess LFP (not shown). The pronounced east-west gradient of U_{10m} and *d* excess across Greenland during the NAO+ phase could warrant further investigation, since higher surface winds are in general expected to be associated with higher *d* excess due to stronger kinetic effects. This is different in regions of strong air-sea humidity contrasts, such as the Mediterranean, where sea spray reduces the strong kinetic effects during evaporation, and therefore lowers the *d* excess [*Gat et al.*, 2003]. As a caveat, we are aware that a direct comparison of SWING ECHAM4 data and ERA-40 data relies on the assumption that the evaporation conditions of the two data sets are at least roughly similar on a monthly timescale. This requirement to be fully met would however require ECHAM4 to be nudged with ERA-40 wind fields.

3.3. Initial Condensation Conditions

[39] Initial condensation (section 2.1) generally occurs north of the moisture source areas for the two NAO phases [*Sodemann*, 2006]. During both NAO phases a maximum of initial condensation is located at the southeastern slope of Greenland, probably in association with orographic cloud formation (not shown). During NAO− months, condensation occurs over a considerably broader area compared to the NAO+ months, which is in agreement with the more southeasterly moisture source regions during the negative phase.

[40] The histogram of the initial condensation temperatures for all precipitating air parcels shows a marked variability with the NAO (Figure 3b): mean T_{cnd} shifts from −2.2 ± 7.1°C for NAO+ to 3.8 ± 6.8°C for NAO− conditions (ΔT_{cnd} = 6.0 K). Thereby, the distribution is

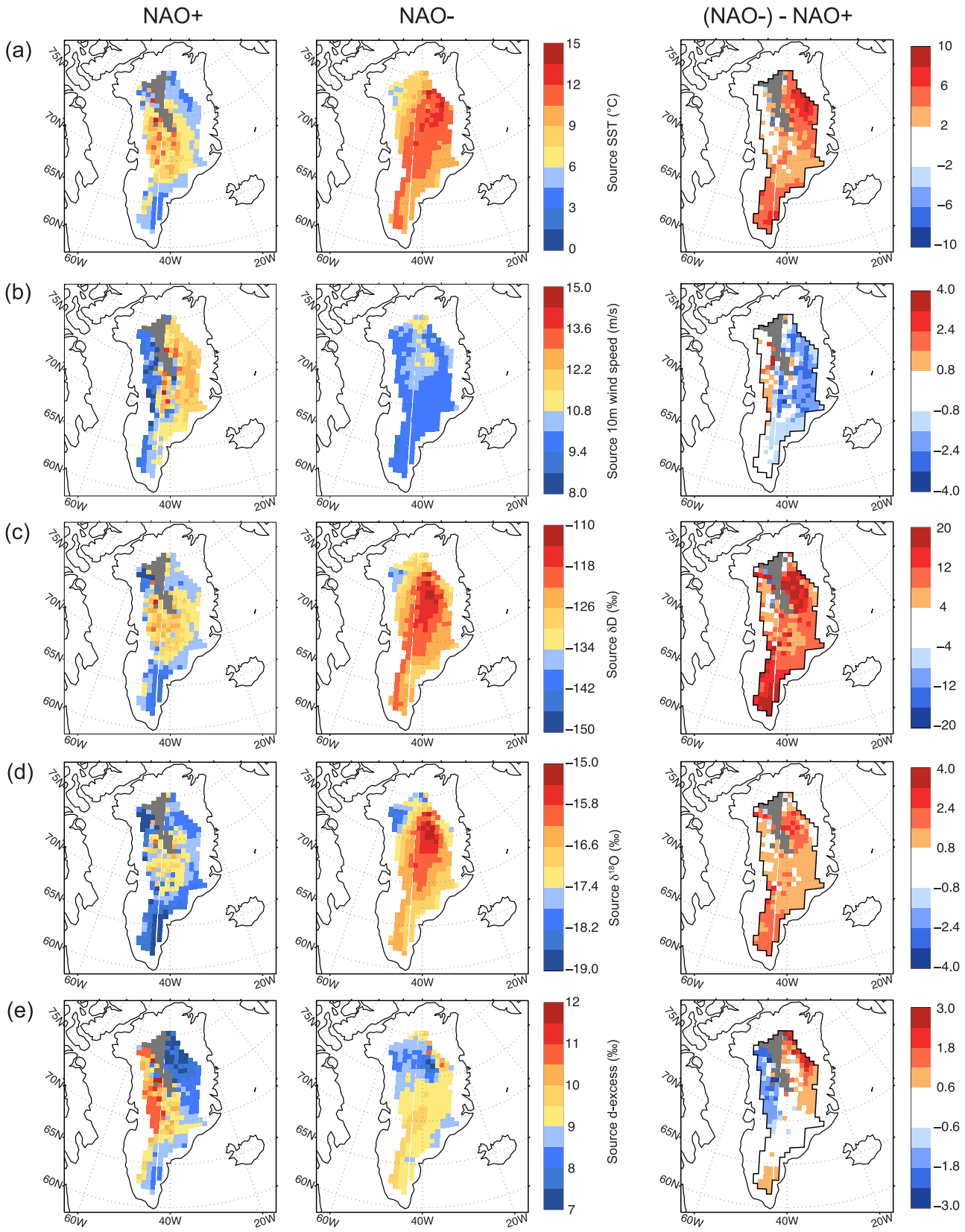

Figure 4. Evaporation conditions of moisture precipitating in Greenland diagnosed from the ERA-40 reanalysis data and the SWING database. Shown are Lagrangian forward projections onto the respective precipitation site, weighted by the precipitation amounts. (a) SST (°C), (b) U_{10m} (m s^{-1}), (c) δD (‰), (d) δ^{18}O (‰), and (e) *d* excess (‰). Areas with very little to no precipitation (less than 50 precipitation events with in total <0.01 mm d^{-1}) are masked in gray.

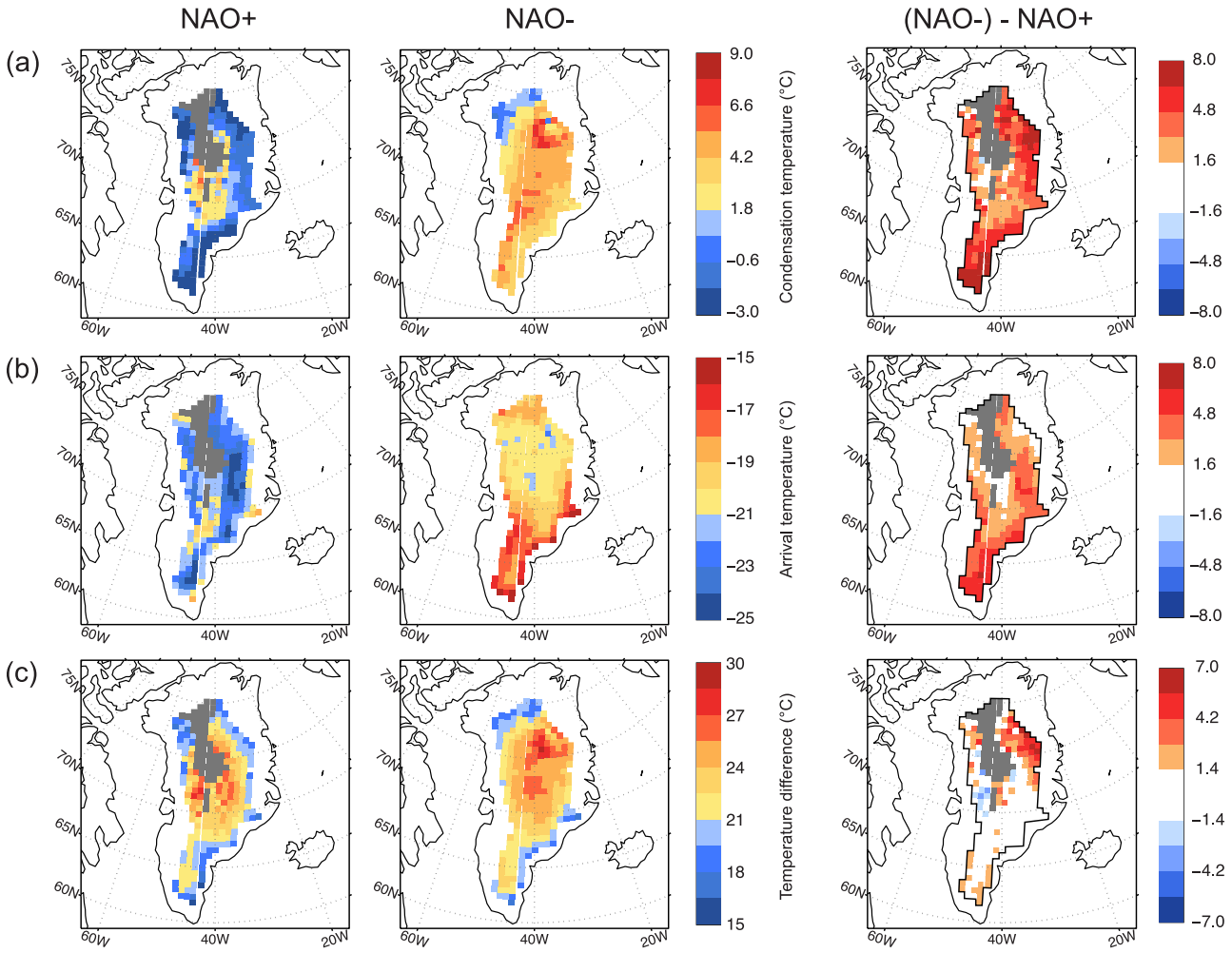

Figure 5. Lagrangian forward projections of the diagnosed conditions of condensation temperatures and arrival temperatures of the precipitation above Greenland, weighted by the respective precipitation amount. (a) Initial condensation temperature T_{cnd} (°C), (b) cloud arrival temperature T_{arr} (°C), (c) temperature difference T_{dif} (K). Gray areas are as in Figure 4.

shifted rather uniformly. This is the case despite the source area during the NAO+ phase being smaller, probably because condensation occurs in an area with a larger latitudinal air temperature gradient. Considering the LFPs of T_{cnd}, regional mean values range between −3°C to 3°C for the NAO+ and 0°C to 8°C for the NAO− phase (Figure 5a). The regional patterns of the forward projected T_{cnd} are again similar to those of the SST (Figure 4a) and the moisture source latitudes (SSW08). During the NAO− phase, anomalously cool T_{cnd} are diagnosed in the northwest of the Greenland plateau (Figure 5a, middle), compared to the corresponding forward projection for SST. The average condensation pressure p_{cnd} is ∼925 ± 61 hPa (corresponding to ∼1000 m a.s.l.) during both phases of the NAO (not shown).

3.4. Cloud Arrival Conditions

[41] Figure 3c shows a strong NAO dependence of the precipitating air parcels' arrival temperature in the clouds over Greenland (T_{arr}): while during NAO+ months the mean value is −22.2 ± 3.9°C, T_{arr} shifts to on average 4.2 K warmer conditions during the NAO− phase (−18.0 ± 4.4°C). Again, the distribution is shifted rather uniformly. In both NAO phases, the pattern of T_{arr} shows an influence of the Greenland orography (Figure 5b): cooler arrival temperatures are found at higher regions, probably due to cloud formation at higher altitudes above sea level. The mean arrival pressure of the moisture above Greenland (∼660 ± 64 hPa) is almost invariant with the NAO (not shown). However, cloud arrival temperatures are remarkably colder during the NAO+ phase (Figure 5b, left). These colder arrival temperatures during NAO+ months correspond to colder midtropospheric temperatures in the Greenland area compared to the NAO− phase (not shown). Note that the joint shift of T_{cnd} and T_{arr} to warmer conditions during the NAO− phase (and vice versa) implies that isotope fractionation occurs in a different range of temperatures (from T_{cnd} = −2.2 ± 7.1 to T_{arr} = −22.2 ± 3.9°C for NAO+, from T_{cnd} = 3.8 ± 6.8 to T_{arr} = −18.0 ± 4.4°C for NAO−).

[42] The temperature difference $T_{dif} = T_{arr} - T_{cnd}$ reflects the temperature range over which isotopic fractionation takes place. The corresponding LFP (Figure 5c) shows that in the interior of the ice sheet T_{dif} is larger than at the slope

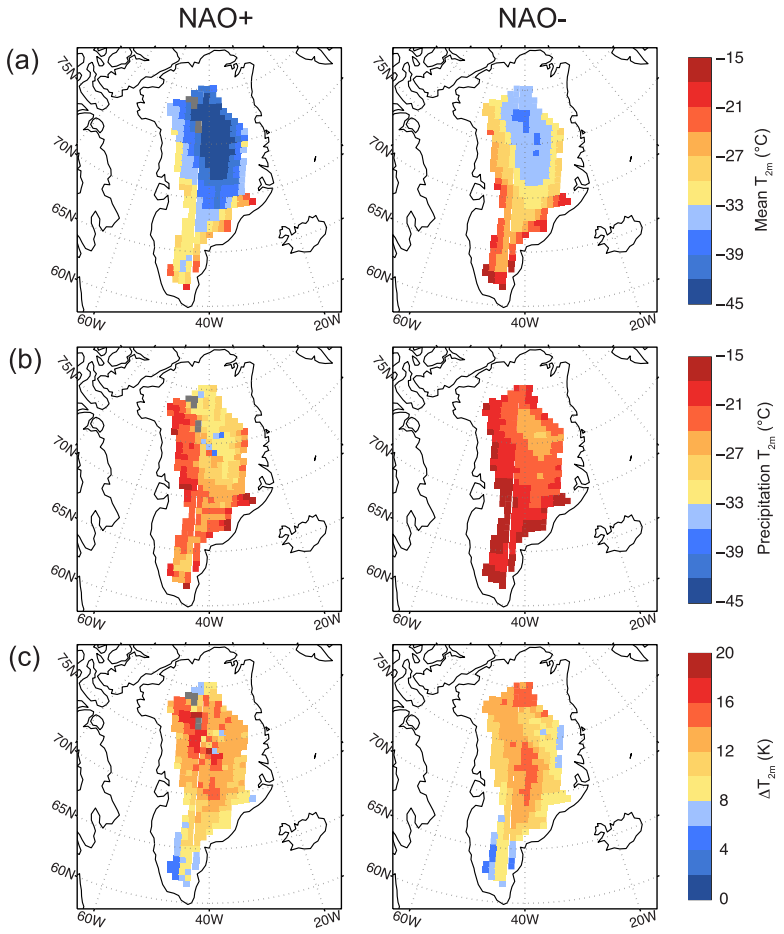

Figure 6. Mean 2 m air temperatures (T_{sfc}) over Greenland (a) for the 10-monthly mean (°C) and (b) on precipitation days only (°C). (c) Difference between precipitation days and monthly mean 2 m air temperatures (ΔT_{sfc}, K). Gray areas mark regions were no precipitation was diagnosed.

(~25°C versus ~20°C). Interestingly, despite the very different evaporation, condensation, and arrival conditions, the range and regional distribution of T_{dif} are quite similar for both NAO phases. The comparatively small NAO variability of T_{dif} (mean shifts from 20.0 ± 7.1°C to 21.8 ± 7.1°C) hence suggests that the NAO variation of moisture source SST and midtropospheric temperatures over Greenland occur in phase. The histogram of the temperature difference (Figure 3d) reveals that the highest values of T_{dif} are more frequent during the NAO− phase. Therefore, the potential for intense fractionation should be somewhat larger during the NAO− phase. The corresponding NAO variability plot shows that this effect is strongest in the very northeast of the Greenland plateau (Figure 5c, right).

3.5. Precipitation Temperatures

[43] The isotope-temperature relationship relates a mean surface temperature to the stable isotope composition of precipitation. Physically, however, the isotopic composition of precipitation is influenced by the cloud temperature during arrival, rather than mean surface temperature. In this section, we compare the temperature conditions at the surface and at cloud level during our study period.

[44] In comparison to typical monthly mean surface temperatures measured during winter on the Greenland ice sheet (e.g., ~−33°C to −43°C at Summit [*Shuman et al.*, 1996]) the mean arrival temperatures of moisture above Greenland found here appear rather warm. However, our diagnosed T_{arr} are recorded at cloud level, and only during precipitation events. While this is also the temperature that is relevant for the isotopic fractionation, it can be substantially different compared to monthly or seasonal mean temperatures, which are dominated by cold and dry conditions. During the advection of midlatitude disturbances, 2 m temperatures were observed to increase strongly near Summit, by as much as 20 K on a daily timescale [*Loewe*, 1936; *Shuman et al.*, 1996].

[45] To quantify the difference of our diagnosed arrival and surface temperatures to the winter mean conditions, ERA-40 2 m temperatures over the Greenland plateau are compared for all winter days and for days with precipitation only during the considered months (Figure 6). The winter mean T_{sfc} is −36.7 ± 5.7°C (−29.5 ± 5.4°C) during the NAO+ (NAO−) phase (Figure 6a). Near the Summit region, the ERA-40 winter mean temperatures compare favorably with those reported by *Shuman et al.* [1996]. For precipitation events only, T_{sfc} are considerably warmer (Figure 6b). Here, the mean is −25.5 ± 4.3°C for the NAO+ and −20.3 ± 3.3°C for the NAO− phase. Over the central region of the plateau, the difference to mean conditions amounts to

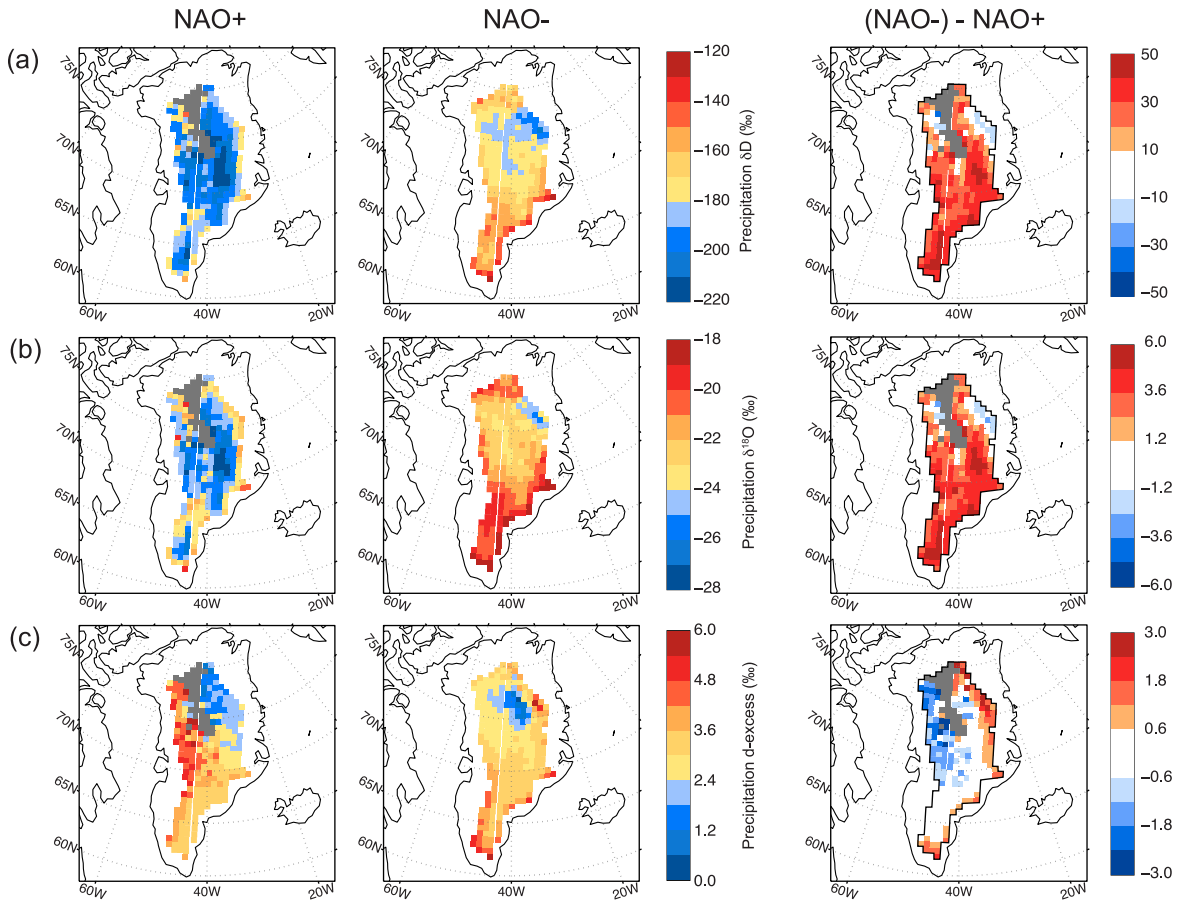

Figure 7. Isotopic composition of Greenland winter precipitation derived from calculations with the MCIM model. (a) δD (‰), (b) δ^{18}O (‰), and (c) d excess (‰). Gray areas are as in Figure 4.

$\sim$14 K. The pattern of the T_{sfc} increase during precipitation periods is very similar for the two NAO phases (Figure 6c). An exception are the anomalously warm northern regions during NAO− months (see section 4.1).

[46] An additional reason for the warmer temperatures diagnosed here is that high-latitude boundary layers are typically dominated by a strong temperature inversion. During advection of moist and warm air the inversion layer is removed. It is not known how well the ERA-40 model simulates this inversion in high-latitude boundary layers.

[47] The temperature differences between mean and precipitation conditions emphasize that the temperatures which determine the extent of isotopic distillation at cloud level and on the synoptic timescale are substantially different from monthly or annual mean conditions at the surface. The importance of this finding for the δ–T relationship is discussed in the next section.

4. Simulated Isotopic Composition of Greenland Precipitation

4.1. Results From MCIM

[48] The MCIM model was applied for calculating isotopic distillation of water vapor on the way from its source area to Greenland according to the diagnosed parameters as presented in the previous section. Figures 7a and 7b show the resulting δD and δ^{18}O in Greenland winter precipitation. Mean isotope ratios are -187 ± 49‰ (-157 ± 48‰) for δD and -23.8 ± 6.2‰ (-20.0 ± 5.9‰) for δ^{18}O during the NAO+ (NAO−) phase ($\Delta\delta$D = 30.5‰, $\Delta\delta^{18}$O = 3.8‰). This is about twice the variability than in the initial isotopic composition at the water vapor source regions (section 3.2 and Figures 4c and 4d). Isotopic NAO variability is rather uniform over the Greenland plateau (Figures 7a and 7b, right). The exception is again an area in the northeast of the plateau. There, isotopic depletion during NAO− months is very similar to, or even higher than during the NAO+ months. This anomaly is probably linked to the larger T_{dif} (or fractionation potential) in this region (Figure 5c).

[49] It is interesting to examine the simulated NAO variability of δ^{18}O in regions where deep ice cores have been retrieved previously. At a grid point near the drilling location of Dye-3 (65.18°N, 45.83°W) $\Delta\delta^{18}$O = 3.71‰ are simulated. Near the central Greenland location Crête (71.12°N, 37.32°W) simulated NAO variability is relatively high (4.56‰). Lower variability is detected at the sites GRIP (72.35°N 38.30°W) and NorthGRIP (75.10°N 42.32°W) with 2.12‰ and 3.53‰, respectively. Near the future drilling site NEEM (77.50°N 50.90°W) reversed (-3.51‰) NAO variability is simulated. It would be insightful to compare the simulated variability with actual data from these ice cores or nearby snow pits. In general, because of firn diffusion and postdeposition effects, the simulated isotope variability should be higher than diagnosed from

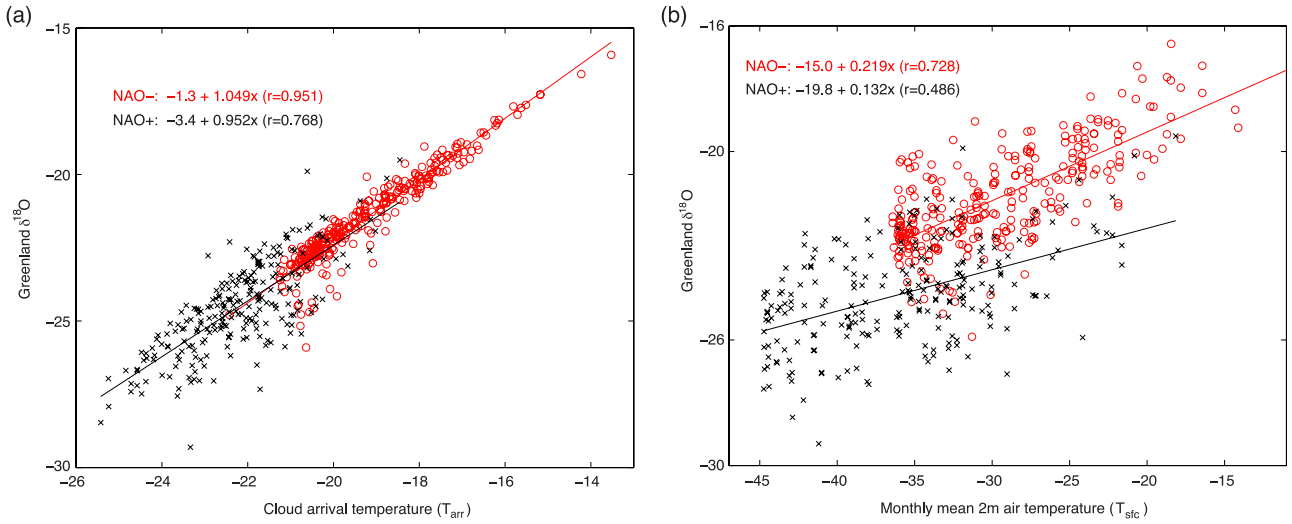

Figure 8. Correlation of modeled NAO phase mean of δ^{18}O (‰) in precipitation over Greenland with (a) cloud arrival temperature during precipitation events (T_{arr}, °C) and (b) mean 2 m air temperature (T_{sfc}, °C) for the NAO+ phase (crosses) and the NAO− phase (circles). One data point is for one location on the calculation grid, averaged over the respective NAO phase. Lines are the corresponding linear regressions with correlation coefficient r as given in each panel.

observations [*Johnsen*, 1977; *Cuffey and Steig*, 1998; *Bolzan and Pohoja*, 2000]. Note also that the simulated variability gets increasingly uncertain with decreasing accumulation.

[50] The areas most suitable for NAO reconstructions from stable isotopes appear to be different from the areas which are best suited for NAO reconstructions from ice core accumulation records (SSW08). For reconstructions based on isotopes, in addition to a strong NAO variability of the isotopic composition itself, accumulation should be high during both, NAO+ and NAO− winters to facilitate the extraction of seasonal isotope data. Figures 7a and 7b suggest that areas particularly suitable for NAO reconstructions from stable isotopes are located south of 65°N, and in the central eastern Greenland plateau.

[51] The LFP pattern of the initial isotopic composition (Figures 4c and 4d) is completely overprinted by the isotopic fractionation during moisture transport. The patterns of δD and δ^{18}O in precipitation closely resemble those of the arrival temperature, also for the NAO variability plots (Figures 7a and 7b, right). This suggests a strong imprint of the range of temperatures during fractionation, in particular the coldest occurring temperatures, on the final isotopic composition. If so, the NAO variability of stable isotope ratios in Greenland would reflect the corresponding atmospheric temperature anomalies in the North Atlantic region [*van Loon and Rogers*, 1978; *Sodemann*, 2006]. This is also suggested by a correlation of NAO phase mean modeled δ^{18}O with the moisture arrival temperature T_{arr} (Figure 8a). Data for both NAO phases spread along a regression line of ~1.0‰ K^{-1}. Minimum and maximum T_{arr} are shifted by ~4–5 K for the two NAO phases. While this correlation argues for a strong imprint of T_{arr} on the final isotopic composition, it does not exclude other possible influences (see section 5.2).

[52] When the $\delta-T$ slope is calculated using the winter mean 2 m temperatures over Greenland from the ERA-40 data (not weighted with precipitation), the two regression slopes decrease differentially (Figure 8b). Besides increased scatter, the NAO+ slope (0.13‰ K^{-1}) is only about 2/3 that of the NAO− slope (0.22‰ K^{-1}). In comparison with estimates for the $\delta-T$ slope which are typically derived for annual mean values, our results are smaller than the global slope reported by *Dansgaard* [1964] and the annual mean Greenland slope by *Johnsen et al.* [1989] (0.67‰ K^{-1}), and also lower than the results from *Shuman et al.* [1995] based on automatic weather station data for Summit (0.46‰ K^{-1}), the station-based estimates reported by *White et al.* [1997] (0.35‰ K^{-1}), and the glacial-interglacial slope given by *Masson-Delmotte et al.* [2006] (0.33‰ K^{-1}). Because of the large scatter, comparison of the slopes without considering the confidence intervals is however somewhat ambiguous. The different slopes for the NAO+ and NAO− months are due to changes in the precipitation distribution over the Greenland plateau with the NAO: the high-altitude areas receive less precipitation during NAO+ months, which in the monthly mean emphasizes the colder dry periods. Accordingly, the most depleted data points shift more strongly along the temperature axis than along the isotope axis. Hence, the submonthly precipitation pattern influences the spatial $\delta-T$ slope. It may be conjectured that the precipitation seasonality influences the isotope-temperature relationship by similar processes [*Steig et al.*, 1994; *Jouzel et al.*, 1997; *Krinner and Werner*, 2003].

[53] The d excess in precipitation during NAO+ months ranges on average between 1–6‰, and shows a clear W–E gradient toward lower values over the Greenland plateau (Figure 7c). During NAO− months, a similar range of values but with a more S–N oriented gradient is apparent. The mean shifts only by 0.6‰ from 3.1 ± 3.8‰ during NAO+ to 3.7 ± 3.3‰ during NAO− months. Regional changes can be as large as 3‰, for instance in the NE of the plateau (Figure 7c, right). Interestingly, the d excess increases with NAO index along the western edge of the

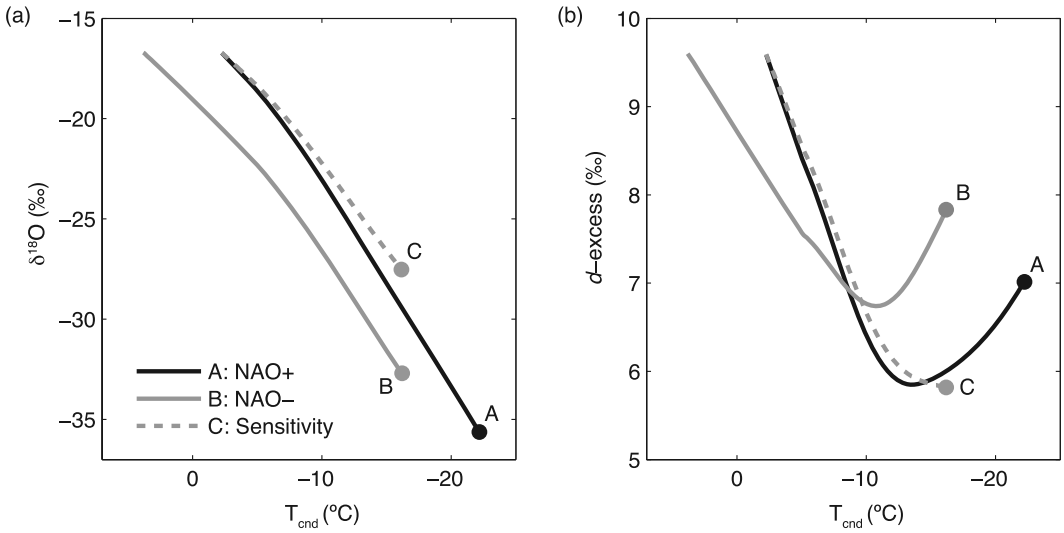

Figure 9. Sensitivity of simulated isotopic composition of the water vapor to condensation temperature for (a) δ^{18}O and (b) *d* excess. End points of the fractionation are marked with a circle. Curve A shows a NAO+ example, temperature range −2.2 to −22.2°C. Curve B shows a NAO− example, temperature range 3.8 to −16.2°C. Curve C shows sensitivity to condensation temperature, temperature range −2.2 to −16.2°C. For all curves, initial δ^{18}O (δD) is −16.7‰ (−124‰), and pressure decreases from 950 to 660 hPa. Curve C is discussed in section 5.1.

plateau, while the reverse applies on the eastern side. The strongest reversal occurs along a west-east transect from ∼73°N to ∼77°N. A comparison with isotope measurements along this transect could clarify if such a reversal is indeed present in nature.

[54] Compared to the initial composition of the water vapor, the simulated precipitation values of *d* excess are ∼6‰ lower, except for the south of Greenland, where the difference is weaker (∼3‰) (Figure 4e). In the MCIM model the main influence on *d* excess during transport, and hence a possible explanation for the shift to lower *d* values, is the linear parameterization of kinetic fractionation effects related to ice supersaturation in mixed phase clouds [*Ciais and Jouzel*, 1994; *Masson-Delmotte et al.*, 2005b]. The spatial pattern of *d* excess for the two NAO phases bears some resemblance with the initial values (Figure 4e), in particular over the northern half of the Greenland ice sheet. This suggests that winter *d* excess variability could partly reflect the variability of the source regions, but one that does not directly translate into source region SST.

[55] Another influence on the *d* excess could originate from equilibrium fractionation, namely from transport at different temperature levels. The ratio of the equilibrium fractionation coefficients decreases slightly with increasing NAO phase, which also reduces the *d* excess. This is supported by idealized fractionation calculations using MCIM (Figure 9). Two sensitivity calculations were carried out over the same temperature range (20 K), but starting at 6.8 K displaced initial condensation temperatures: Curve A represents conditions similar to the mean NAO+ conditions as diagnosed here, while curve B exemplifies NAO− conditions. Despite identical initial δ^{18}O composition, curve B has an ∼2‰ higher isotope ratio at the end of the distillation pathway (Figure 9a). The *d* excess takes a markedly different evolution in the two experiments (Figure 9b). In this example, the final *d* excess is about 0.8‰ lower for curve A (NAO+ case) than for curve B (NAO− case), as a result of equilibrium fractionation alone.

[56] The spatial heterogeneity of the simulated *d* excess in Figure 7c could at least partially be caused by different temperatures during moisture advection. It is possible that the systematically higher levels of present-day *d* excess observed in ice cores from the NorthGRIP site compared to GRIP data are related to similar processes [*Masson-Delmotte et al.*, 2005a, 2005b].

4.2. Comparison With Observational Data

[57] In a first attempt to relate the model results to observational data, the simulated δ^{18}O is compared to stable isotope data from the Alphabet ice cores (see section 2.4). For three selected winters, it is examined how the absolute values and the NAO variability of the modeled isotope ratios compare with the winter season ice core data.

[58] Observed mean δ^{18}O at the Alphabet cores is more depleted for the winter 1983/1984 (−38.4 ± 2.9‰) than for the winters 1964/1965 (−35.1 ± 2.1‰) and 1968/1969 (−36.3 ± 2.3‰) (Table 1). Since winter 1983/1984 was in the neutral to positive NAO phase, this season is considered as an example for the stable isotope signature during NAO+ conditions. The winters 1964/1965 and particularly 1968/1969 where dominated by neutral to negative NAO, and are hence considered as examples for NAO− conditions. According to precipitation from the ERA-40 reanalysis, the isotopic composition of the winter precipitation of 1964/1965 and 1968/1969 are probably dominated by February 1965 and January 1969, respectively. The estimated mean NAO variability in the observations is $\Delta\delta^{18}O = 2.76‰$ (calculated as the mean difference between winter 1983/1984 and the two winters 1964/1964 and 1968/1969).

[59] The simulated precipitation-weighted δ^{18}O variability agrees both qualitatively (more depletion during NAO+ winters) and quantitatively (mean modeled $\Delta\delta^{18}$O is 4.0‰

Table 1. Comparison of Observed Winter Season Stable Isotope Data ($\delta^{18}O_{Obs}$) From the Alphabet Cores (70.63–71.76°N; 35.82–39.62°W, 3018–3138 m a.s.l.) With MCIM Isotope Model Results ($\delta^{18}O_{MCIM}$) for Corresponding Grid Points[a]

Year	Month	NAO Index	$\delta^{18}O_{Obs}$ (‰)	$\delta^{18}O_{MCIM}$ (‰)
1983	Dec	0.4		
1984	Jan	4.1	−38.4 ± 2.9	−25.5 ± 4.1
1984	Feb	1.7		(N/A)
1964	Dec	−0.2		
1965	Jan	−0.3		
1965	Feb	−5.1	−35.1 ± 2.1	−21.7 ± 5.2
1968	Dec	−3.6		(N/A)
1969	Jan	−4.3	−36.3 ± 2.3	−21.3 ± 5.1
1969	Feb	−4.0		

[a]Mean and standard deviation of model results were calculated from 9 grid points and weighted by the respective precipitation amounts from the ERA-40 reanalysis. N/A designates months which were not included in the model calculations.

versus observed 2.76‰) with observations (Table 1). The larger variability in the model results is consistent with the expected smoothing of isotope values due to firn diffusion. The correspondence between modeled and observed variability indicates that the factors which influence the NAO variability of the isotopic composition of precipitation are indeed captured by the model calculations. In section 5.2 it is attempted to disentangle the roles of the various factors on the isotope NAO variability.

[60] For all three winters the simulated absolute $\delta^{18}O$ values are however substantially less depleted (∼13–14‰) than the observations (Table 1). Hence for this site at least, isotopic fractionation is considerably underestimated when MCIM is applied with diagnosed fractionation conditions and water vapor initialized from isotope GCM data. The possible reasons for this offset are discussed in section 5.1.

[61] Currently, no δD data are available from the Alphabet cores, hence no direct comparison between modeled and observed δD and d excess can be performed. *Hoffmann et al.* [1998a] found winter mean values for δD of −290‰ (values ranging from −315‰ to −275‰) in a high-resolution ice core section from GRIP, spanning the years 1970–1980. This translates into a similar lack of depletion in our results for the δD (∼110‰) as for the $\delta^{18}O$.

[62] In a study based on data from the GISP2 core (72.6°N, 38.5°W), *Barlow et al.* [1993] investigated the dependency of winter δD (defined by the δD minimum) and d excess with extreme values of the NAO. For an ice core section spanning the years 1840–1970, d excess was on average 9.4 ± 1.6 for NAO+ and 8.7 ± 2.0 for NAO− winters, in agreement with expectations for warmer moisture sources during NAO− winters. The d excess values from the MCIM model are only about half as large, even though in the initial conditions d excess was around 9‰ (Figure 4e). From the MCIM results we find some indication for similar NAO variability with about 1‰ larger values during the positive NAO phase in the region of GISP2 (Figure 7c, right). However, the annual maxima and minima of d excess in Greenland ice cores are in Northern Hemisphere fall and spring [*White et al.*, 1988; *Johnsen et al.*, 1989]. Hence, a more in-depth comparison of modeled and observed d excess should include these seasons, or even cover a full seasonal cycle.

[63] For the d excess at GRIP, *Hoffmann et al.* [1998a] found a winter mean of 5‰ (values ranging between 2–10‰), which corresponds reasonably to the d excess at the central plateau found here (∼3‰, Figure 7c). Along a transect of shallow ice cores crossing the ice divide along ∼47°W, 69.5°N to 28°W, 72.5°N, winter mean d excess for a site just east of the ice divide [*Fischer et al.*, 1995, site T47] ranged between ∼2–11‰. Interestingly, annual averages of d excess where distributed rather uniformly along the transect at about 12.7‰ with a seasonal amplitude of 4‰. While we do not report annual mean values here, our results suggest that winter variability of d excess with the NAO would be largest (and reversed) along a Greenland transect at ∼77°N (Figure 7c).

5. Discussion

[64] In the following, two aspects of this study are discussed in more detail: (1) the reasons for the offset in stable isotope values calculated with the MCIM model in comparison to observations and (2) the factors which contribute to the simulated NAO variability of the stable isotope signal.

5.1. Offset Between Modeled and Observed Isotopic Levels

[65] The substantially underestimated depletion of the simulated isotopic composition could be due to a number of uncertainties, which are discussed below.

5.1.1. Uncertainties of the Moisture Source Diagnostic

[66] One possible source of uncertainties are the initial isotope values extracted from the ECHAM4 simulations. Both the ECHAM4 simulation and ERA-40 rely on observational monthly mean SST data. Since the isotopic composition in the lowest model layer is in close correspondence with the SST (not shown), it is unlikely that systematic biases were introduced here. This may however be less clear for kinetic effects during evaporation, which more strongly depend on day-to-day atmospheric conditions, such as surface winds and relative humidity [*Gat et al.*, 2003].

[67] The initial isotopic composition of the water vapor relies on the evaporation parameterizations in ECHAM4. In a sensitivity experiment where MCIM was run with initial isotope values derived from the global closure of *Merlivat and Jouzel* [1979], on average ∼8‰ less depleted values were found for $\delta^{18}O$ than with the GCM initialization [*Sodemann*, 2006]. The NAO variability calculated with the global closure initialization however was in a similar range as with the GCM initialization. This argues for the isotope GCM initial conditions being at least closer to reality than the global closure equation. Direct measurements of the isotopic composition of the water vapor at the moisture sources would be required to rigidly verify the initial isotopic composition.

[68] In comparison with previous studies, we diagnose relatively cool moisture source temperatures (average values 5–10°C compared to 15–20°C [*Jouzel and Koster*, 1996] or 22–26°C [*Johnsen et al.*, 1989]). It should be emphasized again that previous studies often considered annual mean moisture source conditions, while we focus on the winter season only. Support for moisture sources during winter north of ∼35°N (i.e., in regions with relatively cold

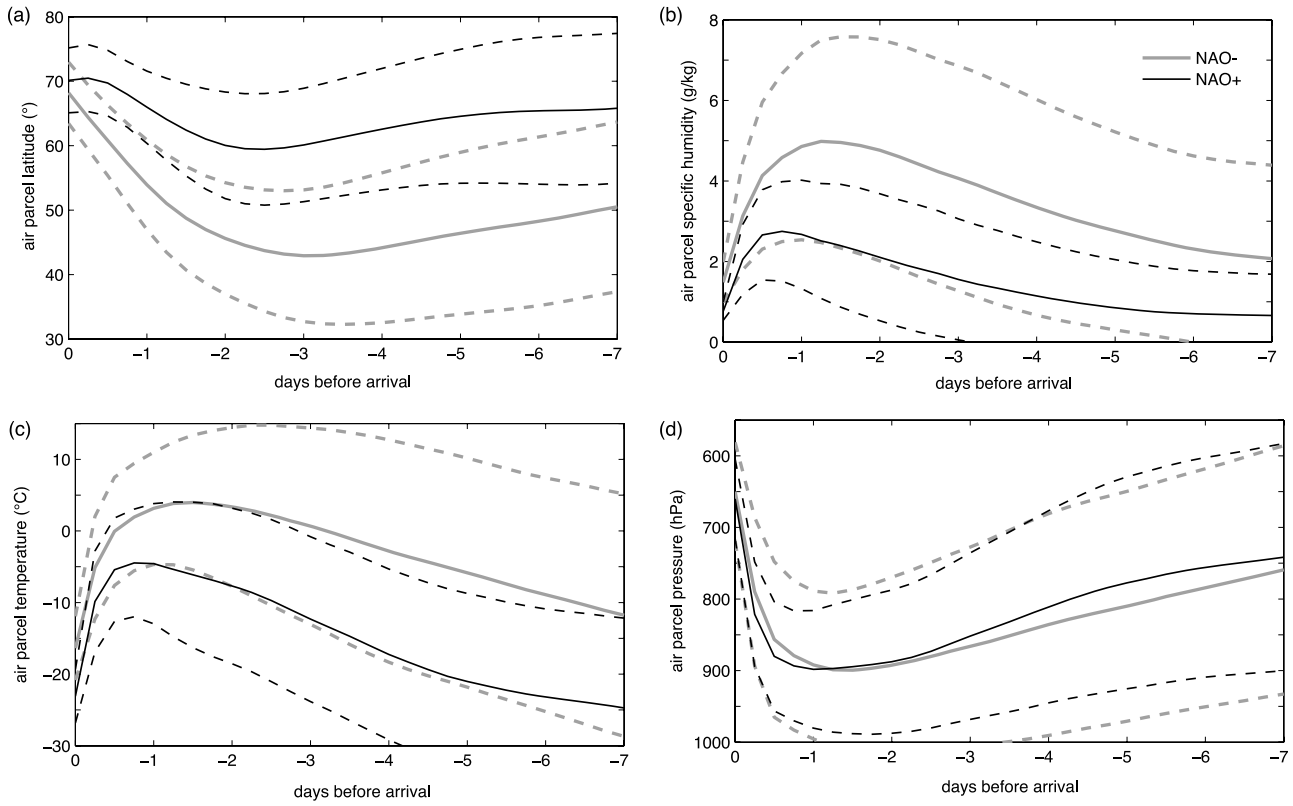

Figure 10. Precipitation-weighted mean (solid) and standard deviation (dashed) for various quantities traced along air parcel trajectories to Greenland during the NAO+ months (black) and NAO− months (gray). Only the last 7 days before arrival over the ice sheet of the 20-day backward trajectories are shown. (a) Latitude (°), (b) specific humidity (g kg^{-1}), (c) air temperature (°C), and (d) pressure (hPa) of the air parcels.

SSTs) is also provided from considering meridional cross sections of mean isentropes in the North Atlantic during winter (not shown). Further support for the northerly latitudes of the moisture sources diagnosed here is provided by NAO phase mean conditions along trajectories (Figure 10). During the last 7 days before arrival in Greenland, substantial differences are present in the mean air parcel latitude between the NAO+ and NAO− months. While the variability is large, southernmost locations are typically reached about 2–3 days before arrival (Figure 10a). The mean moisture content of the air parcels however increases after this most southerly excursion (Figure 10b). This is consistent with on average warming air masses as they descend to levels of higher pressure (lower altitude) (Figures 10c and 10d), which increases the probability for moisture uptake in the marine boundary layer. Thus, Figure 10 illustrates that air parcels leading to precipitation over Greenland do not simply transport moisture from their southernmost latitude to Greenland, but that significant amounts of moisture are picked up during their poleward journey. Within the framework of the ERA-40 data set, the identified moisture source locations are consistent with the physics of evaporation, and it appears unlikely that our method for moisture source attribution contains a substantial artificial bias toward too local moisture sources. In the future, a direct comparison to an Eulerian moisture tracking method could further confirm that this is the case.

[69] The initial condensation locations are one of the more uncertain aspects of the diagnosed moisture transport parameters. The current definition as the first occurrence of saturation along a trajectory after the last identified moisture source location could shift the condensation regions too close to Greenland (since a trajectory might be associated with several uptakes, see SSW08). This would then lead to a too late onset of isotopic fractionation, and a systematic underestimation of isotopic distillation.

[70] Figure 9 gives some indication of the sensitivity of the simulated isotope ratios to the condensation temperatures. Curve C is the same as curve B, except for a 6.8 K colder condensation onset temperature. The shift in initial condensation temperature leads to 8‰ weaker depletion in $\delta^{18}O$ and 1.2‰ lower d excess due to the shorter distillation path. Note also that the fractionation is considerably different than for A at the same temperatures, as the fractionation proceeds along a different adiabat. This illustrates the potentially large sensitivity of the calculation results to initial condensation temperature. A definite answer on the sensitivity to this parameter can however only be expected from fractionation calculations that exactly follow the fractionation conditions along diagnosed trajectories.

[71] The arrival temperatures of moisture above Greenland diagnosed from the ERA-40 data are unlikely to show a large systematic offset. To explain 10‰ of the isotopic offset would require a midtropospheric warm bias of ~8 K. Atmospheric temperatures over Greenland in the ERA-40 reanalysis are constrained by several radiosonde stations distributed along the coast of Greenland. Assimilation of

these data should lead to reasonable agreement between observed and modeled midtropospheric temperatures, even in such a generally data-sparse region. A quantitative check would however require the comparison of radiosonde profiles from the Greenland ice sheet with ERA-40 data.

5.1.2. Uncertainties in the Comparison With Observations

[72] One principal limitation in the comparison of our model results with observations concerns the lack of isotope measurements during snowfall events in Greenland. Some uncertainty is also introduced from assigning isotope values from ice cores to a specific season, since no mass balance monitoring or direct precipitation isotope measurements are in place on the Greenland ice sheet. Postdepositional effects such as wind erosion and isotopic diffusion in the firn layers add further uncertainty.

[73] In Antarctica, clear-sky precipitation contributes up to 50% of the annual accumulation, and can be associated with very low isotope ratios [*Ekaykin et al.*, 2002, 2004; *Masson-Delmotte et al.*, 2008]. For Greenland, no estimate for the contribution of clear-sky precipitation to total precipitation is available from the literature. It is therefore currently not possible to asses whether potentially highly depleted diamond dust contributes in sufficient amounts to accumulation in some parts of Greenland, and hence contributes to the lower than modeled isotope ratios.

[74] The Greenland orography affects the lifting of air masses as they are advected onto the ice sheet. Steeper slopes and higher altitudes in the real orography compared to the ERA-40 model may lead to stronger isotopic fractionation [*Smith et al.*, 2005]. The quantitative impact of this effect is unknown, but could possibly be large. In the vicinity of the Alphabet site, an orographic isotope gradient of 0.6‰/100 m is observed. However, with an altitude difference of only about ~100 m between the ERA-40 orography and the real world at the Alphabet sites, less than 1‰ depletion for $\delta^{18}O$ can be explained by this direct orographic effect.

[75] Small-scale topographic influences are also apparent within the Alphabet ice core array. Ice cores to the east of the ice divide are on average ~1.5‰ more depleted than ice cores further to the west, where accumulation is also considerably larger [*Clausen et al.*, 1988]. *Fischer et al.* [1995] attributed a similar east-west difference around Crête partially to gradual orographic distillation of air masses advected from the west, but also to different moisture sources on both sides of the ice divide. On the basis of the between-core variance, such small-scale effects could explain 1–2‰ of the lack of isotopic depletion.

[76] The various influences of orographic effects suggest that the site chosen for this initial comparison might not be ideal. Lower-altitude sites that are less affected by rain shadowing and that receive more precipitation, for instance in southern Greenland, could be better suited for future seasonal comparisons. To a certain degree, however, orographic effects are likely to be important at all (Greenland) ice core sites.

5.1.3. Uncertainties in the Isotope Distillation Modeling

[77] An important factor which could lead to a lack of isotopic depletion in the MCIM results is the distillation trajectory. The air parcel trajectories diagnosed from reanalysis data can include several cycles of condensation. They also could prevail at different temperature ranges than the idealized $p-T$ trajectory used in MCIM (Figure 1). The diagnosed mean air parcel temperature and pressure conditions in Figure 10 however confirm that the fractionation parameters diagnosed from the trajectories and supplied to MCIM agree well with the simple weighted mean. On average, air parcels reach their highest pressure 1–2 days before arrival over the ice sheet (Figure 10d). This coincides also with the warmest temperatures and highest moisture content during the last 7 days of the moisture transport (Figures 10b and 10c). Thereafter, air parcels cool rapidly and decrease in specific humidity as they are dynamically and orographically lifted onto the ice sheet. These mean characteristics are remarkably similar to the MCIM distillation trajectories which correspond to the diagnosed moisture transport parameters. Individual air parcels can however show markedly stronger cooling rates than the mean, and than the linear path in MCIM. This may have strong influences on microphysical processes in the clouds, in particular with respect to supersaturation [*Schmidt et al.*, 2005].

[78] By calculating the fractionation separately for each uptake event, we treat a potentially nonlinear process as linear. While this seems valid as a first approximation, the full transport and fractionation history of an air mass could be considered better by running MCIM as a box model along diagnosed distillation trajectories. Such an approach has recently been introduced by *Helsen et al.* [2004]. In their Lagrangian approach based on the MCIM model and reanalysis trajectories, both for the whole of Antarctica [*Helsen et al.*, 2007] and for single sites [*Helsen et al.*, 2004, 2005], simulated levels of isotopic depletion are in good absolute correspondence with data near the coasts, but underestimate total depletion in the Antarctic interior. Their calculations however rely heavily on atmospheric monthly mean isotope data from isotope GCMs throughout the moisture transport process. While we only extract the initial isotopic composition of the evaporating moisture from isotope GCM data, their method performs "isotopic recharge" [*Kavanaugh and Cuffey*, 2003] every time moisture increase is detected in an air parcel. It therefore appears that the approach of *Helsen et al.* [2004] currently takes an intermediate position between isotope GCMs and fully Lagrangian isotope box model calculations.

[79] Isotopic recharge relates to the problem of mixing, which is currently not addressed in our methodology. Here, about ~20% of the water vapor enters air parcels at locations above the boundary layer, and another ~14% of the moisture originates from unknown sources (SSW08). Depleted water vapor from the free troposphere could reduce simulated isotopic values as it is mixed into rising air parcels. From linear mixing with highly depleted ambient vapor (e.g., $\delta^{18}O$ of −40 to −50‰ for winter storm clouds in the middle troposphere [*Smith*, 1992]), about 50–80% of mixing would be required to reach 13‰ more depleted $\delta^{18}O$ values. This simple estimate clearly exceeds the amount of moisture without attributed sources according to the methodology of SSW08. Nevertheless, mixing should be considered as a potentially important process which lowers isotope levels in a Lagrangian framework. In future studies, Lagrangian particle dispersion models could be

Table 2. Comparison of the Greenland Mean Temperature Parameters and Isotope Composition at the Moisture Sources From the ECHAM4 Isotope GCM ($\delta^{18}O_{src}$) and the Modeled Greenland Ice Sheet Mean ($\delta^{18}O_{MCIM}$)

	NAO+ (°C)	NAO− (°C)	Δ_T (K)
SST	5.0 ± 6.5	10.0 ± 6.7	+5.0
T_{cnd}	−2.2 ± 7.1	3.8 ± 6.8	+6.8
T_{arr}	−22.2 ± 4.0	−18.0 ± 4.4	+4.2
T_{dif}	20.0 ± 7.1	21.8 ± 7.1	−1.8
	NAO+ (‰)	NAO− (‰)	Δ_δ (‰)
$\delta^{18}O_{src}$	−18.4 ± 2.9	−16.7 ± 2.8	+1.7
$\delta^{18}O_{MCIM}$	−23.8 ± 6.2	−20.0 ± 5.9	+3.8

applied to address the problem of mixing due to turbulence and convection.

[80] Originally, MCIM was designed to simulate realistic isotope levels for Antarctic conditions [*Ciais and Jouzel*, 1994]. Arrival cloud temperatures were estimated from an empirical relationship between the annual mean surface temperature and the temperature above the inversion (equation (A1)). If this empirical relation is used to calculate the cloud arrival temperature from the mean 2 m air temperature during NAO+ and NAO− winters, between 5 K to 8 K colder moisture arrival temperatures result than diagnosed from the ERA-40 data. If run with such markedly colder (but, for Greenland, unrealistic) cloud arrival temperatures, MCIM simulates 6–10‰ more depleted $\delta^{18}O$ in precipitation. Hence, the difference between the estimated and diagnosed cloud arrival temperatures explains a large share of the isotopic offset in the model results compared to previous studies.

[81] It seems that the original MCIM model implicitly accounted for mixing and other processes by the cooler than diagnosed cloud arrival temperatures. It can only be speculated here which process could lead to the high depletion of the Greenland precipitation observed in nature. For example, lifting of the air masses as they approach the orographic barrier of the Greenland plateau leads to large cooling rates during the orographically forced ascent. This could cause intense fractionation over a relatively short horizontal distance, and thereby lead to strong gradients in the isotopic composition of the surface precipitation, which cannot be captured by our model approach. Furthermore, ice crystals with very low isotope ratios from aloft could deplete underlying air masses because of reevaporation and cloud seeding. There clearly is a need for improved Lagrangian Rayleigh-type models with detailed microphysical parameterizations and the consideration of mixing processes. At the same time, detailed isotope measurements of both, water vapor and precipitation, at high latitudes are highly needed. Such information would also help to better constrain the parameterization of isotopic fractionation in isotope GCMs.

[82] In the context of this work, the most important point of this discussion is that none of the above factors seems to be systematically affected by the NAO. Therefore, despite the strong lack of isotopic depletion in absolute numbers, it remains possible to attempt a meaningful interpretation of the simulated NAO variability of isotopes in Greenland precipitation.

5.2. Relative Importance of Fractionation Temperatures

[83] It is now attempted to disentangle how the various factors contribute to the modeled (and assumedly also the observed) NAO variability of the water isotopes, in particular $\delta^{18}O$. The Greenland mean changes of moisture source SST, T_{cnd}, T_{arr}, and T_{dif} with the NAO are compared qualitatively to the change in modeled isotopic composition (Table 2). Temperature differences Δ_T and isotope differences Δ_δ between the two NAO phases are used as indicators that are defined such that positive (negative) values denote less (more) isotopic depletion during NAO+ than during NAO−. Note that all mean values are significantly different (two-sided Student's t test at the $\alpha = 5\%$ level).

[84] Cooler Greenland mean moisture source SSTs during NAO+ compared to NAO− months coincide with more depleted initial isotope values (Table 2). Colder average T_{cnd} and T_{arr} during NAO+ months signify that fractionation takes place at a lower temperature range, which leads to stronger depletion. T_{dif} in contrast is smaller during NAO+ months, probably because of a shorter transport distance in the NAO+ phase. This provides a smaller temperature range for fractionation than for NAO− months. In brief, the NAO variability of Greenland isotopes is caused by more depletion due to cooler sources and a cooler temperature range during NAO+ than during NAO− months. The slightly smaller T_{dif} during NAO+ months reduces the larger depletion potential, but only to a minor extent.

[85] Since the initial isotopic composition of the water vapor at the moisture source is known, a tentative quantification of the source and transport influences can be accomplished. SST differences of 5.0 K are associated with a change of 1.7‰ in the initial conditions of $\delta^{18}O$. Considering the modeled average Δ_δ over Greenland of 3.8‰, this implies that the combined transport effects contribute another 2.1‰ to the variability. Accordingly, the simulated NAO variability of δD and $\delta^{18}O$ in Greenland precipitation is a combined signal, with roughly equal contributions from moisture source and air temperature changes. The NAO variability is hence enhanced, compared to atmospheric temperature changes or moisture source changes only.

[86] Different regions of Greenland experience various degrees of moisture source variability with the NAO (SSW08). Hence, regional differences of the isotopic NAO variability can be composed of varying moisture source and air temperature changes. A particular interesting region in this respect is the north of the Greenland ice sheet. Data from the new ice core drilling project NEEM and toward the east of NorthGRIP would be particularly suitable to test our results. For a fully independent assessment, it would in addition be very important to gather atmospheric stable water isotope data from evaporation sites in the North Atlantic.

6. Summary and Conclusions

[87] We applied a new Lagrangian moisture source diagnostic to study the interannual variability of the isotopic composition of winter precipitation over the Greenland ice sheet. The atmospheric conditions relevant for isotopic distillation, which water vapor experiences during transport

to Greenland, vary strongly with the NAO. The temperature range during which fractionation takes place is shifted to cooler conditions during NAO+ months compared to NAO− months. The SST of the moisture sources changes strongly, because of the shifted location of the moisture sources. Along with warmer SSTs during NAO− than NAO+ months, the evaporating moisture becomes initially less depleted of stable isotopes.

[88] On the basis of the diagnosed moisture transport conditions, the stable water isotopes δD and δ^{18}O in Greenland precipitation were simulated with a Rayleigh-type isotope fractionation model. An initial comparison with seasonal stable isotope data from an array of ice cores in central Greenland showed that modeled isotope levels were systematically too high. The difference between observed and simulated levels of isotopic depletion are largely caused by the fact that cloud arrival temperatures which were previously estimated from an empirical relation are considerably colder than what we diagnose from the ERA-40 data during precipitation events. This finding emphasizes that earlier assumptions relating cloud condensation temperatures to surface temperatures are invalid on a subseasonal timescale. It also suggests that the submonthly frequency of precipitation events is crucial for determining which air temperatures are actually reflected in the stable isotope signal. The intermittency of precipitation, and its seasonality, together with detailed mass balance studies, should therefore be a part of future efforts to understand the current seasonality of the isotopic composition of Greenland precipitation.

[89] In contrast to the absolute values, the interannual variability of simulated isotope levels in precipitation in central Greenland agreed well with observations. The variability of precipitation δD and δ^{18}O with the NAO can be understood as a combined effect of source region changes and changes in atmospheric fractionation temperatures, with about equal contributions. The joint variability in moisture sources and atmospheric temperatures amplifies the interannual variability of the stable isotopes, compared to impacts from only one of the factors. It is speculated that this enhancement of the interannual variability due to atmospheric circulation changes could also be relevant for understanding rapid changes recorded in Greenland ice cores during past climates.

[90] Because of the high spatial resolution, our results are useful for interpreting differences in the interannual variability between ice cores from different locations on the Greenland ice sheet, as well as for the selection of new ice core drilling sites. The findings of this study suggest that areas particularly suitable for NAO reconstructions from stable isotopes in ice cores are located south of 65°N and in the central eastern Greenland plateau. In these areas, (model) precipitation occurs during both NAO+ and NAO− winters, facilitating the extraction of seasonal isotope data from firn and ice cores, while at the same time modeled isotopic NAO variability is high. These areas are not necessarily identical with those most suitable for NAO reconstructions from accumulation records.

[91] For the secondary isotopic parameter d excess, we found no evidence for a direct role of the moisture source SST in the interannual variability during winter. This finding is however limited by the many uncertainties surrounding the parameter d excess, both with respect to observational data and model parameterizations. One test for the current understanding of isotope physics would be a comparison with data along a west-east transect in central Greenland to validate if the d excess NAO variability indeed reverses from east to west. Clearly, additional spatial coverage of stable isotope measurements of δD and δ^{18}O at the moisture source areas and of Greenland precipitation is required to validate and to refine both current isotope GCMs and Lagrangian isotope models. Stable water isotopes could thus be used more effectively to constrain the realism of the modeled hydrological cycle.

Appendix A: Adjusted Lapse Rates in the MCIM Model

[92] Isotopic fractionation was calculated from the Rayleigh-type fractionation model MCIM. Originally, MCIM calculates the isotopic fractionation along a $p-T$ trajectory that is specified by the moisture source SST and the annual mean surface temperature at a location on the ice sheet. The cloud arrival temperature is thereby estimated from an empirical equation derived for Antarctic conditions, which relates the annual mean surface temperature T_{sfc} to the temperature at cloud height by

$$T_{\mathrm{arr}} = 0.67 \cdot T_{\mathrm{sfc}} + 1.2 \tag{A1}$$

[93] In order to feed our diagnosed moisture transport conditions to the model, we calculated adjusted lapse rates and RH at the surface so that condensation onset and the subsequent fractionation would occur at the diagnosed moisture transport conditions. Initial compositions of the water vapor at condensation onset were taken from the ECHAM4 isotope GCM. Instead of the empirically estimated cloud arrival temperatures, those derived from the Lagrangian moisture transport diagnostic were used.

[94] Input values for the calculation of the adjusted input parameters were the moisture source temperature (SST), the condensation temperature T_{cnd}, and the pressure at condensation level p_{cnd}. Output values were an adjusted relative humidity at the surface RH_a, and an adjusted lapse rate lr_a. In detail, the calculation proceeded as follows:

[95] 1. Calculate the saturation vapor pressure e_c^* for T_{cnd}:

$$e_c^* = 6.1078 \cdot \exp\left(a \frac{T_{\mathrm{cnd}} - 273.16}{T_{\mathrm{cnd}} - b}\right) (\mathrm{hPa}) \tag{A2}$$

where for ice a = 21.8745584 and b = 7.66, for water a = 17.2693882 and b = 35.86.

[96] 2. Find a condensation altitude z_c which corresponds to the diagnosed condensation pressure p_{cnd} assuming a US standard atmosphere.

[97] 3. Calculate the adjusted lapse rate lr_a from the vertical temperature gradient between the surface and condensation level:

$$lr_a = \frac{T_{\mathrm{cnd}} - T_{\mathrm{sfc}}}{z_c} \left(\mathrm{K\ km^{-1}}\right) \tag{A3}$$

[98] 4. Calculate the adjusted relative humidify at the surface RH_a^* corresponding to the water vapor pressure at the surface e_0^* using equation (A2):

$$RH_a = e_c^*/e_0^*. \quad \text{(A4)}$$

[99] **Acknowledgments.** MeteoSwiss is gratefully acknowledged for providing access to the ECMWF ERA-40 reanalysis data. Martin Werner provided help with and access to the SWING database. This study was partly funded by the Swiss National Fund's NCCR Climate programme. V. M. D. acknowledges the support of the Agence Nationale de la Recherche for the LSCE. B. M. V. thanks the Carlsberg Foundation for funding. Two anonymous reviewers are acknowledged for their insightful comments.

References

Appenzeller, C., J. Schwander, S. Sommer, and T. Stocker (1998a), The North Atlantic Oscillation and its imprint on precipitation and ice accumulation in Greenland, *Geophys. Res. Lett.*, *25*(11), 1939–1942.

Appenzeller, C., T. Stocker, and M. Anklin (1998b), North Atlantic Oscillation dynamics recorded in Greenland ice cores, *Science*, *282*, 446–449.

Armengaud, A., R. D. Koster, J. Jouzel, and P. Ciais (1998), Deuterium excess in Greenland snow: Analysis with simple and complex models, *J. Geophys. Res.*, *103*(D8), 8947–8953.

Barlow, L. K., J. W. C. White, R. G. Barry, J. C. Rogers, and P. M. Grootes (1993), The North Atlantic Oscillation signature in Deuterium and Deuterium excess signals in the Greenland ice sheet project 2 ice core, 1840–1970, *Geophys. Res. Lett.*, *24*(20), 2901–2904.

Barlow, L. K., J. C. Rogers, M. C. Serreze, and R. G. Barry (1997), Aspects of climate variability in the North Atlantic sector: Discussion and relation to the Greenland Ice Sheet Project 2 high-resolution isotopic signal, *J. Geophys. Res.*, *102*(C12), 26,333–26,344.

Bolzan, J. F., and V. A. Pohoja (2000), Reconstruction of the undiffused seasonal oxygen isotope signal in central Greenland ice cores, *J. Geophys. Res.*, *105*(C9), 22,095–22,106.

Boyle, E. A. (1997), Cool tropical temperatures shift the global d18O-T relationship: An explanation for the ice core d18O-borehole thermometry conflict?, *Geophys. Res. Lett.*, *24*(3), 273–276.

Charles, R. D., D. Rind, J. Jouzel, R. D. Koster, and R. G. Fairbanks (1994), Glacial-interglacial changes in moisture sources for Greenland: Influences on the ice core record of climate, *Science*, *263*, 508–511.

Ciais, P., and J. Jouzel (1994), Deuterium and oxygen 18 in precipitation: Isotopic model, including mixed cloud processes, *J. Geophys. Res.*, *99*(D8), 16,793–16,803.

Ciais, P., J. W. C. White, J. Jouzel, and J. R. Petit (1995), The origin of present-day Antarctic precipitation from surface snow deuterium excess data, *J. Geophys. Res.*, *100*(D9), 18,917–18,927.

Clausen, H. B., N. S. Gundestrup, S. J. Johnsen, R. Bindschadler, and J. Zwally (1988), Glaciological investigations in the Crête area, central Greenland: A search for a new deep-drilling site, *Ann. Glaciol.*, *10*, 10–15.

Craig, H., and L. I. Gordon (1965), Deuterium and oxygen 18 variations in the ocean and the marine atmosphere, in *Stable Isotopes in Oceanographic Studies and Paleotemperatures*, edited by E. Tongiorgi, pp. 9–130, Lab. di Geol. Nucl., Cons. Naz. delle Ric., Pisa, Italy.

Cuffey, K., and G. Clow (1997), Temperature, accumulation, and ice sheet elevation in central Greenland through the last deglacial transition, *J. Geophys. Res.*, *102*(C12), 26,383–26,396.

Cuffey, K. M., and E. J. Steig (1998), Isotopic diffusion in polar firn: Implications for interpretation of seasonal climate parameters in ice-core records, with emphasis on central Greenland, *J. Glaciol.*, *44*(147), 273–284.

Cuffey, K. M., G. D. Clow, R. B. Alley, M. Stuiver, E. D. Waddington, and R. W. Saltus (1995), Large Arctic temperature-change at the Wisconsin-Holocene glacial transition, *Science*, *270*(5235), 455–458.

Dahl-Jensen, D., K. Mosegaard, N. Gundestrup, G. D. Clow, S. J. Johnsen, A. Hansen, and N. Balling (1998), Past temperatures directly from the Greenland ice sheet, *Science*, *282*, 268–271.

Dansgaard, W. (1964), Stable isotopes in precipitation, *Tellus*, *16*, 436–468.

Dansgaard, W., et al. (1993), Evidence for general instability of past climate from a 250-kyr ice-core record, *Nature*, *364*(6434), 218–220.

Delmotte, M., V. Masson, J. Jouzel, and V. I. Morgan (2000), A seasonal deuterium excess signal at Law Dome, coastal eastern Antarctica: A southern ocean signature, *J. Geophys. Res.*, *105*(D6), 7187–7197.

Ekaykin, A. A., V. Y. Lipenkov, N. I. Barkov, J. R. Petit, and V. Masson-Delmotte (2002), Spatial and temporal variability in isotope composition of recent snow in the vicinity of Vostok station, Antarctica: Implications for ice-core record interpretation, *Ann. Glaciol.*, *35*, 181–186.

Ekaykin, A. A., V. Y. Lipenkov, I. N. Kuzmina, J. R. Petit, V. Masson-Delmotte, and S. J. Johnsen (2004), The changes in isotope composition and accumulation of snow at Vostok station, East Antarctica, over the past 200 years, *Ann. Glaciol.*, *39*, 569–575.

EPICA Community Members (2004), Eight glacial cycles from an Antarctic ice core, *Nature*, *429*, 623–628.

Fischer, H., D. Wagenbach, M. Laternser, and W. Haeberli (1995), Glacio-meteorological and isotopic studies along the EGIG line, central Greenland, *J. Glaciol.*, *41*(139), 515–527.

Fujita, K., and O. Abe (2006), Stable isotopes in daily precipitation at Dome Fuji, East Antarctica, *Geophys. Res. Lett.*, *33*, L18503, doi:10.1029/2006GL026936.

Gat, J. R., B. Klein, Y. Kushnir, W. Roether, H. Wernli, R. Yam, and A. Shemesh (2003), Isotope composition of air moisture over the Mediterranean Sea: An index of air-sea interaction pattern, *Tellus, Ser. B*, *55*, 953–965.

Helsen, M. M., R. S. W. van de Wal, M. R. van den Broeke, E. R. T. Kerstel, V. Masson-Delmotte, H. A. J. Meijer, C. H. Reijmer, and M. P. Scheele (2004), Modelling the isotopic composition of snow using backward trajectories: A particular precipitation event in Dronning Maud Land, Antarctica, *Ann. Glaciol.*, *39*, 293–299.

Helsen, M. M., R. W. van de Wal, M. van den Broeke, D. van As, H. Meijer, and C. Reijmer (2005), Oxygen isotope variability in snow from western Dronning Maud Land, Antarctica and its relation to temperature, *Tellus, Ser. B*, *57*, 423–435.

Helsen, M. M., R. S. W. van de Wal, and M. R. van den Broeke (2007), The isotopic composition of present-day Antarctic snow in a Lagrangian atmospheric simulation, *J. Climate*, *20*(4), 739–756, doi:10.1175/JCLI4027.1.

Hoffmann, G., M. Stiévenard, J. Jouzel, J. W. C. White, and S. J. Johnsen (1998a), Deuterium excess record from central Greenland, modelling and observations, in *International Symposium on Isotope Techniques in the Study of Past and Current Environmental Changes in the Hydrosphere and the Atmosphere*, pp. 591–602, Int. At. Energy Agency, Vienna, Austria.

Hoffmann, G., M. Werner, and M. Heimann (1998b), Water isotope module of the ECHAM atmospheric general circulation model: A study on timescales from days to several years, *J. Geophys. Res.*, *103*(D14), 16,871–16,896.

Hoffmann, G., J. Jouzel, and V. Masson (2000), Stable water isotopes in atmospheric general circulation models, *Hydrol. Processes*, *14*, 1385–1406.

Johnsen, S. J. (1977), Stable isotope homogenisation of polar firn and ice, *IAHS Publ.*, *118*, 210–219.

Johnsen, S. J., W. Dansgaard, and J. W. C. White (1989), The origin of Arctic precipitation under present and glacial conditions, *Tellus, Ser. B*, *41*, 452–468.

Johnsen, S. J., D. Dahl-Jensen, W. Dansgaard, and N. Gundestrup (1995), Greenland palaeotemperatures derived from GRIP bore hole temperature and ice core isotope profiles, *Tellus, Ser. B*, *47*, 624–629.

Johnsen, S. J., H. B. Clausen, K. M. Cuffey, G. Hoffmann, J. Schwander, and T. Creyts (2000), Diffusion of stable isotopes in polar firn and ice: The isotope effect in firn diffusion, in *Physics of Ice Core Records*, edited by T. Hondoh, pp. 121–140, Hokkaido Univ. Press, Sapporo, Japan.

Joussaume, S., R. Sadourny, and C. Vignal (1986), Origin of precipitating water in a numerical simulation of July climate, *Ocean Air Interact.*, *1*, 43–56.

Jouzel, J., and R. D. Koster (1996), A reconsideration of the inital conditions used for stable water isotope models, *J. Geophys. Res.*, *101*(D17), 22,933–22,938.

Jouzel, J., and L. Merlivat (1984), Deuterium and oxygen 18 in precipitation, modelling of the isotopic effects during snow formation, *J. Geophys. Res.*, *89*, 11,749–11,757.

Jouzel, J., L. Merlivat, J. R. Petit, and C. Lorius (1983), Climatic information over the last century deduced from a detailed isotopic record in the South Pole snow, *J. Geophys. Res.*, *88*, 2693–2703.

Jouzel, J., et al. (1997), Validity of the temperature reconstruction from water isotopes in ice cores, *J. Geophys. Res.*, *102*(C12), 26,471–26,487.

Jouzel, J., M. Stiévenard, S. J. Johnsen, A. Landais, V. Masson-Delmotte, A. Sveinbjornsdottir, F. Vimeux, U. von Grafenstein, and J. W. C. White (2007), The GRIP deuterium-excess record, *Quat. Sci. Rev.*, *26*, 1–17.

Kavanaugh, J. L., and K. M. Cuffey (2003), Space and time variation of $\delta^{18}O$ and δD in Antarctic precipitation revisited, *Global Biogeochem. Cycles*, *17*(1), 1017, doi:10.1029/2002GB001910.

Krinner, G., and M. Werner (2003), Impact of precipitation seasonality changes on isotopic signals in polar ice cores: A multi-model analysis,

Earth Planet. Sci. Lett., *216*, 525–538, doi:10.1016/S0012-821X(03)00550-8.

Krinner, G., C. Genthon, and J. Jouzel (1997), GCM analysis of local influences on ice core d signals, *Geophys. Res. Lett.*, *24*(22), 2825–2828.

Loewe, E. (1936), The Greenland ice cap as seen by a meteorologist, *Q. J. R. Meteorol. Soc.*, *62*, 359–377.

Masson-Delmotte, V., J. Jouzel, A. Landais, M. Stiévenard, S. J. Johnsen, J. W. C. White, M. Werner, A. Sveinbjornsdottir, and K. Fuhrer (2005a), GRIP deuterium excess reveals rapid and orbital-scale changes in Greenland moisture origin, *Science*, *309*, 118–121, doi:10.1126/science.1108575.

Masson-Delmotte, V., et al. (2005b), Holocene climatic changes in Greenland: Different deuterium excess signals at Greenland Ice Core Project (GRIP) and NorthGRIP, *J. Geophys. Res.*, *110*, D14102, doi:10.1029/2004JD005575.

Masson-Delmotte, V., et al. (2006), Past temperature reconstructions from deep ice cores: Relevance for future climate change, *Clim. Past*, *2*, 145–165.

Masson-Delmotte, V., et al. (2008), A review of Antarctic surface snow isotopic composition: Observations, atmospheric circulation and isotopic modelling, *J. Clim*, in press.

Merlivat, L., and J. Jouzel (1979), Global climatic interpretation of the deuterium-oxygen 18 relationship for precipitation, *J. Geophys. Res.*, *84*(C8), 5029–5033.

Mosley-Thompson, E., C. R. Readinger, P. Craigmile, L. G. Thompson, and C. A. Calder (2005), Regional sensitivity of Greenland precipitation to NAO variability, *Geophys. Res. Lett.*, *32*, L24707, doi:10.1029/2005GL024776.

Noone, D. (2006), Isotopic composition of water vapor modeled by constraining global climate simulations with reanalyes, in *Research Activities in Atmospheric and Oceanic Modelling*, vol. 35, edited by J. Cote, pp. 2–47, World Meteorol. Organ., Geneva, Switzerland.

Noone, D., and I. Simmonds (2002), Annular variations in moisture transport mechanisms and the abundance of δ^{18}O in Antarctic snow, *J. Geophys. Res.*, *107*(D24), 4742, doi:10.1029/2002JD002262.

NorthGRIP Members (2004), High-resolution record of Northern Hemisphere climate extending into the last interglacial period, *Nature*, *431*(7005), 147–151.

Petit, J. R., J. W. C. White, N. W. Young, J. Jouzel, and Y. S. Korotkevich (1991), Deuterium excess in recent Antarctic snow, *J. Geophys. Res.*, *96*, 5113–5122.

Rayner, N. A., D. E. Parker, E. B. Horton, C. K. Folland, L. V. Alexander, D. P. Rowell, E. C. Kent, and A. Kaplan (2003), Global analyses of sea surface temperature, sea ice, and night marine air temperature since the late nineteenth century, *J. Geophys. Res.*, *108*(D14), 4407, doi:10.1029/2002JD002670.

Rogers, J. C., J. F. Bolzan, and V. A. Pohjola (1998), Atmospheric circulation variability associated with shallow-core seasonal isotopic extremes near Summit, Greenland, *J. Geophys. Res.*, *103*(D10), 11,205–11,219.

Rozanski, K., C. Sonntag, and K. O. Münnich (1982), Factors controlling stable isotope composition of European precipitation, *Tellus*, *34*(2), 142–150.

Rozanski, K., L. Aráguas-Aráguas, and R. Gonfiantini (1993), Isotopic patterns in modern global precipitation, in *Climate Change in Continental Isotopic Records*, *Geophys. Monogr. Ser.*, vol. 78, edited by P. K. Swart, J. McKenzie, and S. Savin, pp. 1–37, AGU, Washington, D. C.

Schlosser, E., C. Reijmer, H. Oerter, and W. Graf (2004), The influence of precipitation origin on the delta O-18-T relationship at Neumayer station, Ekstromisen, Antarctica, *Ann. Glaciol.*, *39*, 41–48.

Schmidt, G. A. (1999), Forward modeling of carbonate proxy data from planktonic foraminifera using oxygen isotope tracers in a global ocean model, *Palaeooceanography*, *14*(4), 482–497.

Schmidt, G. A., G. Hoffmann, D. T. Shindell, and Y. Hu (2005), Modeling atmospheric stable water isotopes and the potential for constraining cloud processes and stratosphere-troposphere water exchange, *J. Geophys. Res.*, *110*, D21314, doi:10.1029/2005JD005790.

Schmidt, G. A., A. N. LeGrande, and G. Hoffmann (2007), Water isotope expressions of intrinsic and forced variability in a coupled ocean-atmosphere model, *J. Geophys. Res.*, *112*, D10103, doi:10.1029/2006JD007781.

Shuman, C. A., R. B. Alley, S. Anadakrishnan, J. W. C. White, P. M. Grootes, and C. R. Stearns (1995), Temperature and accumulation at the Greenland Summit: Comparison of high-resolution isotope profiles and satellite passive microwave brightness temperature trends, *J. Geophys. Res.*, *100*(D5), 9165–9177.

Shuman, C. A., M. A. Fahnestock, R. A. Bindschadler, R. B. Alley, and C. R. Stearns (1996), Composite temperature record from the Greenland Summit, 1987–1994: Synthesis of multiple automatic weather station records and SSM/I brightness temperatures, *J. Clim.*, *9*(6), 1421–1428.

Smith, R. B. (1992), Deuterium in North Atlantic storm tops, *J. Atmos. Sci.*, *49*, 2041–2057.

Smith, R. B., I. Barstad, and L. Bonneau (2005), Orographic precipitation and Oregon's climate transition, *J. Atmos. Sci.*, *62*, 177–191.

Sodemann, H. (2006), *Tropospheric Transport of Water Vapour: Eulerian and Lagrangian Perspectives*, *Diss. ETH 16623*, Logos Verlag Berlin, Berlin, Germany.

Sodemann, H., C. Schwierz, and H. Wernli (2008), Interannual variability of Greenland winter precipitation sources: Lagrangian moisture diagnostic and North Atlantic Oscillation influence, *J. Geophys. Res.*, *113*, D03107, doi:10.1029/2007JD008503.

Steig, E. J., P. M. Grootes, and M. Stuiver (1994), Seasonal precipitation timing and ice core records, *Science*, *266*, 1885–1886.

Sturm, K., G. Hoffmann, B. Langmann, and W. Stichler (2005), Simulation of δ^{18}O in precipitation by the regional circulation model REMOiso, *Global Planet. Change*, *19*, 3425–3444.

van Loon, H., and J. C. Rogers (1978), Seesaw in winter temperatures between Greenland and Northern Europe. Part I: General description, *Mon. Weather Rev.*, *106*(3), 296–310.

Vinther, B. M., S. J. Johnsen, K. K. Andersen, H. B. Clausen, and A. W. Hansen (2003), NAO signal recorded in the stable isotopes of Greenland ice cores, *Geophys. Res. Lett.*, *30*(7), 1387, doi:10.1029/2002GL016193.

Vinther, B. M., K. K. Andersen, P. D. Jones, K. R. Briffa, and J. Cappelen (2006), Extending Greenland temperature records into the late eighteenth century, *J. Geophys. Res.*, *111*, D11105, doi:10.1029/2005JD006810.

Werner, M., M. Heimann, and G. Hoffman (2001), Isotopic composition and origin of polar precipitation in present and glacial climate simulations, *Tellus, Ser. B*, *53*, 53–71.

White, J. W. C., S. J. Johnsen, and W. Dansgaard (1988), The origin of Arctic precipitation as deduced from its deuterium excess, *Ann. Glaciol.*, *10*, 219–220.

White, J. W. C., L. K. Barlow, D. Fisher, P. Grootes, J. Jouzel, S. J. Johnsen, M. Stuiver, and H. Clausen (1997), The climate signal in the stable isotopes of snow from Summit, Greenland: Results of comparisons with modern climate observations, *J. Geophys. Res.*, *102*(C12), 26,425–26,439.

V. Masson-Delmotte, LSCE, IPSL, CEA, CNRS, UVSQ, CE Saclay, F-91191 Gif-sur-Yvette, France.

C. Schwierz, Institute for Climate and Atmospheric Science, University of Leeds, Leeds LS2 9JT, UK.

H. Sodemann, Norwegian Institute for Air Research, N-2027 Kjeller, Norway. (harald.sodemann@nilu.no)

B. M. Vinther, Centre for Ice and Climate, Niels Bohr Institute, University of Copenhagen, DK-2100 Copenhagen, Denmark.

H. Wernli, Institute for Atmospheric Physics, University of Mainz, D-55099 Mainz, Germany.